Techno-economic analysis of production of bio-oil from catalytic pyrolysis of olive mill wastewater sludge with two different cooling mechanisms

Muhammad Shoaib Ahmed Khan, Najla Grioui, Kamel Halouani, Riad Benelmir

Techno-economic analysis of production of bio-oil from catalytic pyrolysis of olive mill wastewater sludge with two different cooling mechanisms

Muhammad Shoaib Ahmed Khan[a*], Najla Grioui[b,c], Kamel Halouani[b,c], Riad Benelmir[a]
[a]LERMAB, Faculty of Sciences and Technologies, Université de Lorraine, Vandoeuvre les Nancy, 54506, France
[b]Micro Electro Thermal Systems (UR13ES76), National Engineering School of Sfax, University of Sfax, IPEIS, Road Menzel Chaker km 0.5- PO Box 1172, 3018 Sfax, Tunisia
[c]Digital Research Center of Sfax, Technopole of Sfax, PO Box 275, Sakiet Ezzit, 3021 Sfax, Tunisia

Abstract

A techno-economic analysis of production of bio-oil from catalytic pyrolysis of olive mill wastewater sludge has been performed with two different cooling schemes. The two configurations differ in the manner how the bio-oil vapors are quenched. In scheme-1, a vapor compression refrigeration machine is utilized for condensation of bio-oil vapors while in scheme-2, the vapor compression refrigeration machine is replaced by absorption refrigeration machine. The two schemes are modelled in Aspen Plus which provides mass and energy balances. For techno-economic analysis, Aspen process economic analyzer is employed. The model is first validated against experimental data from lab scale and then upscaled to an industrial scale of 100 tonnes/day wet biomass (93 tonnes/day dry biomass). Results show that the model with absorption refrigeration machine (scheme-2) has a slightly better process efficiency and a lower MFSP compared to the model with compression refrigeration machine (scheme-1). Total anticipated capital investment expenses for scheme-1 and scheme-2, comprising plant fixed capital investment (FCI), start-up, working capital, and interest, are expected to be €22.1 M and €17.5 M, respectively. The equipment costs are based on first quarter of 2021 and the economic life of the project is 20 years. Monte Carlo sensitivity analyses showed that the bio-oil MFSP is most vulnerable to discounted cash flow, income tax and bio-oil yield. The production cost

of bio-oil varies between €2.16/GGE and €6.19/GGE for scheme-1 and €1.78/GGE and €5.01/GGE for scheme-2 when cost parameters are varied within an industrially relevant range. The findings support the viability of producing bio-oil by catalytic fast pyrolysis on a commercial scale.

.

Keywords: Aspen Plus, Process simulation, Catalytic Fast pyrolysis, Fluidized bed, Olive mill wastewater sludge, Techno-economic study

*Corresponding author: muhammad-shoaib-ahme.khan@univ-lorraine.fr

1- Introduction

The olive oil business is vital to the economies of various Mediterranean nations, including Spain, Greece, Turkey, Italy, and Tunisia. However, the extraction of olive oil produces a lot of olive mill wastewater (OMW), which is acidic in nature and pollutes the land and water. OMW is commonly disposed off in surrounding uninhabited places or lakes, where it remains for an extended period of time. Many procedures such as dilution, filtration, and sedimentation have been explored in the past to lessen the negative effects of OMW, but none of them seems to be effective. As a result, it became essential to apply a chemical method to transform it into certain innocuous yet valuable compounds [1]. These transformations can take place in two ways: biochemical and thermochemical [2]. Torrefaction, pyrolysis, and gasification are the three basic types of thermochemical processes [3]. One of the possibilities of treating OMWS is the production of bio-oil through fast pyrolysis.

Under atmospheric pressure, fast pyrolysis is a thermal conversion process that transforms biomass into organic vapors, gases, water, and char in the absence of oxygen. The feedstock qualities are the primary determinants of product yield composition. At medium temperatures (about 400–500°C), fast pyrolysis of OMWS takes place. The organic vapor

55 portion, which is condensed into bio-oil, is the principal product. There is also the production
56 of non-condensable gases, water, and biochar.

57 The main advantage of pyrolysis and combustion is that these processes shrink the
58 large volumes of OMWS [1]. There are four types of pyrolysis in use: slow, intermediate, fast,
59 and flash depending upon operating conditions. The most significant operating parameters
60 which effect the product yields include heating rate, temperature of reactor, biomass particle
61 size and residence time [5,6]. Intermediate pyrolysis (slow heating rates, intermediate solid
62 residence times) is still in its infancy. Recent research has shown that intermediate pyrolysis
63 oil derived from biomass and waste can provide a product oil with superior characteristics that
64 is more comparable to biodiesel and diesel fuels [7]. Pyrolysis produces products in three
65 different forms: solid (char), liquid (bio-oil), and syngas (pyrolytic gas); thus, it is widely used
66 to convert biomass waste to energy [8]. Fast pyrolysis is regarded to be a suitable mechanism
67 for generating clean and high energy content bio-oil from various types of biomass, among
68 other thermochemical techniques [2]. In fast pyrolysis, biomass is heated to elevated
69 temperature in a very limited time. The process is favorable if the bio-oil yield is maximum
70 among other products. [9].

71 The use of the Aspen Plus modeling software in process modeling has grown in recent
72 years. It is a modeling software that calculates a process's physicochemical and biological
73 properties. The tool is popular because it may be used for all phases of the process (solid,
74 liquid, and vapor) [10]. A few recent studies have shown that the simulation tool may be used
75 to analyze pyrolysis experiments and forecast the process yields [11] . The tool is also useful
76 for manipulating pyrolysis process parameters such as heating rate, temperature, solid
77 residence time, feedstock size, and so on.

78 Many simulation studies on different types of biomass such as beachwood [12], empty
79 fruit bench, sawdust and giant miscanthus [13], lignocellulosic feedstock [14], Napier grass

bagasse [15], pinewood [16], pine and forest residues [17], hybrid polar [18], spruce, wheat straw and corn stover [19] have been performed. In these simulation models, the biomass is decomposed into its basic building blocks (cellulose, hemicellulose and lignin) using *RYield* reactor, followed by kinetic reactions in *RCSTR* reactor and then finally secondary reactions in *RYield* reactor. The decomposition of biomass is governed by Power Law type reactions.

$$r = k * T^{n} * e^{-R/RT} \quad (1)$$

Where *r* is the rate of reaction, *k* is pre-exponential factor, *T* is the temperature, *E* is activation energy and *R* is gas law constant. These studies used the particle size distribution less than 2mm and nitrogen was employed as fluidizing gas for pilot plant while non-condensable gases for industrial scale plants. Many researchers used catalyst ZSM-5 and sand as fluidized bed medium [12,20]. The temperature for pyrolysis reactor ranges from 400 to 520°C and bio-oil yield lies in the range of 28%- 64% [12,13,19]. The Aspen Plus model was effectively used to forecast pyrolysis product production and to study the effect of temperature on pyrolysis product output. So far, pyrolysis models which have been studied and developed in Aspen Plus are based on the work of Ranzi et. al. [21] which target the cellulosic biomass. In these studies, the simulation and experimental data were found to be in good agreement, demonstrating that Aspen Plus simulator may be used to forecast the yield of pyrolysis products. The simulation findings also showed that utilizing Aspen Plus, the pyrolysis operating parameters can be successfully adjusted, and the findings may be utilized for experimental testing.

The bio-oil derived from the pyrolysis is acidic in nature, has low energy content, contains oxygenated compounds and high viscosity [22]. Catalysts can be used to improve the characteristics of the bio-oil comparable to diesel. High-molecular-weight compounds are cracked into lower-molecular-weight products during the pyrolysis process. [23]. The catalytic pyrolysis bio-oil is thermally more stable and contains less acidic and oxygenated

104 compounds [24]. In the presence of catalysts, the distribution of pyrolysis products across the
105 solid, liquid, and gaseous phases has been observed to change. Without additional
106 upgradation, biomass catalytic pyrolysis produces useful biofuels such as gasoline and diesel
107 fuel, heating oil, and other monocyclic aromatic hydrocarbons such as benzene, toluene, and
108 xylene [25]. In general, two types of catalysts are utilized in pyrolysis, depending on the
109 chemical nature of the material: acid and base catalysts. Biochar production is normally
110 increased by acidic catalysts, whilst bio-oil production can be increased by base catalysts [26].
111 The products distribution is highly dependent on the nature, quantity of catalyst, and operating
112 conditions of the pyrolysis process [27].
113 Among the pyrolysis catalysts, zeolite-based catalysts are the most frequent. However, the
114 generation of oxygenated molecules decreases while that of aromatic hydrocarbons increases
115 [28]. Few studies have been published on the use of base catalysts in biomass pyrolysis. CaO,
116 MGO, K_2CO_3, and Na_2CO_3 are examples of metal oxides of alkali and alkaline that have
117 shown the potential for catalytic pyrolysis, producing bio-oil with high heating value and
118 lower oxygen compounds [29].
119 The catalysts used in pyrolysis may be classified into three types depending on the method
120 utilized. In the first category, catalyst is mixed with biomass before entering the pyrolysis
121 reactor. The second category deals with the catalyst already placed in the reactor and biomass
122 added after thus making a direct contact. The catalysts for the third category are put into a
123 second reactor, which is placed downstream of the primary reactor. In a study carried out by
124 Dong et. al. [30], the researchers reported a three times more carbon product from two stage
125 catalytic pyrolysis in the presence of light olefins than single stage reactor.
126 Several previous studies report the cost of producing bio-oil via fast
127 pyrolysis [15,17,20,31–34] by varying assumptions for biomass cost, plant capacity, reactor
128 technology, and other variables. Economic analysis of large-scale models was conducted in

Aspen Process Economic Analyzer (APEA) [19]. These studies have estimated the cost of bio-oil to range between €1.75 and €8.67/GGE (€0.014/MJ - €0.07/MJ). Capital cost for the study conducted by Wright et. al. [33] is €166 million for a pyrolysis plant of 2000 tons/day. The economic analysis of a plant of 49 kg/hr Napier grass bagasse indicates that the capital cost is estimated to be €1.77 million and operating cost €0.25 million [15].

In this study, we propose to develop an Aspen Plus model which takes into account the global kinetic parameters for the production of pyrolytic bio-oil from fast pyrolysis of OMWS (catalytic and non-catalytic) and compare the simulation results with the experimental data of Agblevor et. al. [35]. After validation of results, the model is upscaled to commercial scale of 100 tonnes/day and two schemes are proposed. The schemes differ in the way of condensing the bio-oil vapors. In scheme-1, the bio-oil vapors are condensed using a compression refrigeration machine, while in scheme-2, an absorption cooling machine is employed for condensation. Finally, a techno-economic analysis is performed to assess the performance of both schemes on the basis of minimum fuel selling price (MFSP) of bio-oil.

2- Materials and Methods

2.1- Experimental data

Experiments were performed by Agblevor et. al. [35] in Utah State University. Olive mill wastewater sludge (OMWS) was collected from a Tunisian evaporation pond. It is dried at ambient temperature before being ground to a size of around 2 mm. The 160 grams of ground biomass are mixed with 40 grams biochar to make it less sticky. Nitrogen gas at 25°C, 1.01 bar is used as carrier to blow it into the fluidizing bed reactor. The fluidized bed reactor has a diameter of 50 mm and a length of 500 mm. The mixture of ground biomass, biochar and nitrogen is introduced into the pyrolysis reactor at ambient temperature. Nitrogen as fluidizing

gas enters from bottom of pyrolysis reactor at 300°C, 1.02 bar. Catalyst; red mud, is heated at 550°C for five hours before using it in the reactor. The experiment is performed at three different temperatures i.e. 400, 450 and 500°C. Bio-oil, steam and biogas are gaseous products while biochar and red mud are solid products. These are separated in a cyclone kept at 400°C so that bio-oil may not condense at this stage. The gaseous products are then passed through condensers (the first co-flow and the second counter-flow) to condense the bio-oil and water vapors. Water/ethylene glycol mixture at 8°C was used as cold fluid in the condensers (Fig. 2). Bio-oil aerosols, biogas and nitrogen are passed through electrostatic precipitator (ESP) where bio-oil is collected at ambient temperature. The biogas and nitrogen are non-condensable at ambient temperature and pressure and can be used for other purposes.

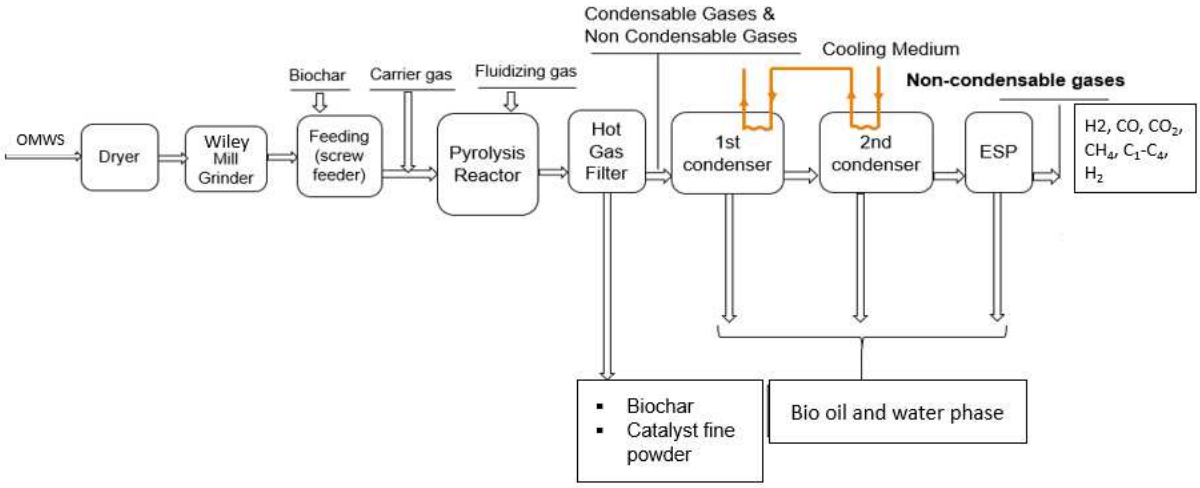

Figure 1. Schematic diagram of pyrolysis of OMWS

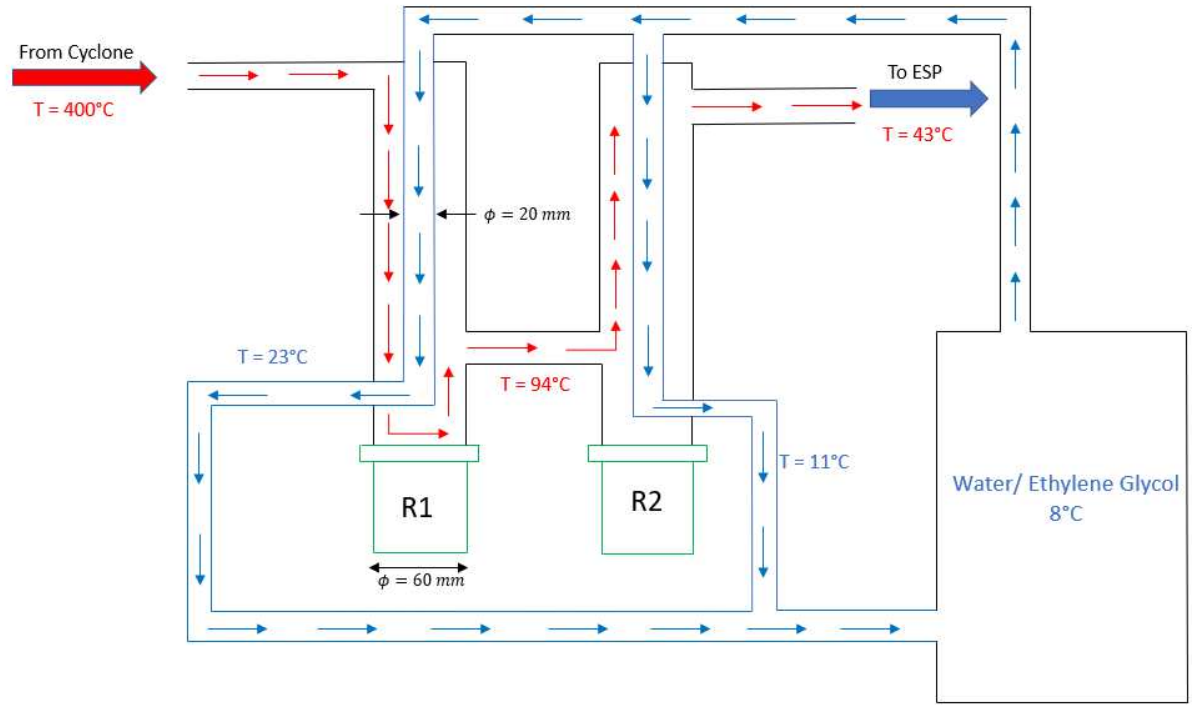

Figure 2. Schematic diagram of shell and tube heat exchanger

Proximate and ultimate analyses of OMWS and biochar are shown in the following Table 1.

Table 1. OMWS and biochar attributes [8]

Attribute	OMWS Biomass	OMWS Biochar
	Proximate analysis (wt. %)	
Moisture	4.08	2.62
Fixed Carbon	22.21	25.43
Volatile Matter	64.43	33.42
Ash	13.36	41.15
	Ultimate analysis (wt.%)	
Carbon	52.89	48.09
Hydrogen	7.16	4.69
Nitrogen	1.96	2.01
Sulfur	0.6	0.15
Oxygen	24.03	3.91
HHV (MJ/kg)	25.64	21.34

Catalyst red mud was used for catalytic pyrolysis while sand was used for non-catalytic pyrolysis. The composition of red mud is given in the following Table 2.

Table 2. Red Mud composition [8]

Metal Oxide	wt. (%)
Fe_2O_3	13.36

Al_2O_3	52.89
SiO_2	7.16
CaO	1.96
TiO_2	0.6
Na_2O	24.03

173

174 *2.2- Simulation model*

175 *2.2.1- Pilot scale*

176 Aspen Plus is a comprehensive powerful tool used by engineers and researchers for
177 a variety of applications including chemical processes, power generation, polymerization,
178 distillation, pharmaceuticals and fertilizers. It contains several tools to calculate mass and
179 energy balance, chemical equilibrium, reaction kinetics and perform optimization studies.
180 Users can benefit from extensive databases thermodynamic models and physical properties
181 to develop complicated and comprehensive processes. Its strength lies in the handling of
182 conventional and non-conventional solids, liquid and gas fuels [36]. Aspen Plus has been
183 used by many researchers for pyrolysis of biomass [37–40].
184 Components in Aspen Plus are divided into two categories: conventional and non-
185 conventional. The molecular structure of conventional components is known, and they may
186 be found in numerous Aspen Plus databanks. Because non-conventional components lack a
187 molecular formula, proximate and ultimate analyses are used to represent them [38].

188 In this work, catalytic and non-catalytic pyrolysis of OMWS is modelled using
189 ASPEN Plus ® software as shown in Figure 3. OMWS and biochar are defined as non-
190 conventional components and described on the basis of proximate and ultimate analysis
191 (Table 1). OMWS, biochar carrier gas and fluidization gas are fed into the fluidized bed
192 reactor where dehydration takes place. After dehydration, feedstock is fed into *RCSTR* (*PYR*)

reactor where biomass is disintegrated into bio-oil, biochar, water and gases according to the global reaction equation (2).

$$OMWS = Bio\ oil + Biochar + Biogas + Water \quad (2)$$

The products exiting the reactor are cooled to 400°C using a simple cooler exchanger (Heater) to keep the products at same temperature as cyclone. Biochar and catalyst are separated in a cyclone and the gaseous products are passed through a first condenser (co-flow HeatX) and cooled to 96°C. The products pass through two separators where bio-oil is separated. About 70% of bio-oil is condensed in the first condenser. The remaining products pass through a second condenser (counter-flow HeatX) and the temperature is further reduced to 42°C. The products pass through two separators where bio-oil and water are separated from the NCG.

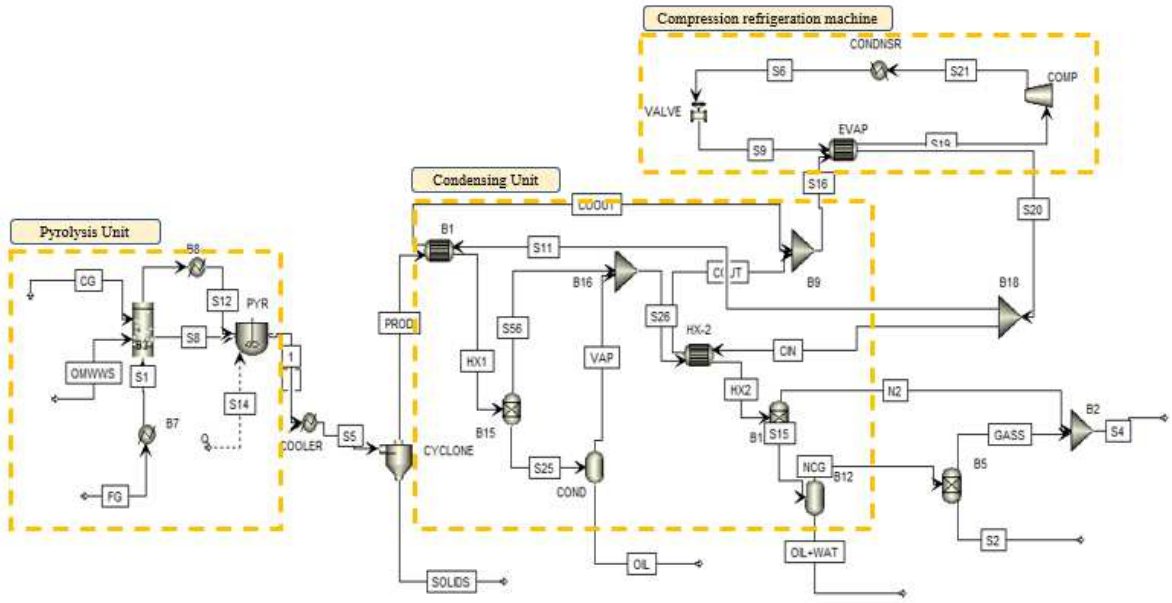

Figure 3. Aspen Plus flowsheet of catalytic fast pyrolysis process of OMWS.

A list of Aspen Plus units and their description is given in Table 3.

Table 3. Aspen Plus unit models

Unit	Description
Fluidized bed reactor	Models the fluidization dynamics and calculates the minimum fluidization velocity and superficial velocity.

RCSTR	Stands for continuous stirred tank reactor. This unit is useful when kinetics of the chemical reaction are known.
Cyclone	Separates solids from gases
HX	Models shell and tube heat exchanger to heat or cool down inlet streams
Comp	Compressor used in compression refrigeration system
Flash2	Executes vapor-liquid equilibrium calculations
Sep	Separates inlet stream components into multiple outlet streams depending upon split fractions or specified flows

2.2.2- Specific heat capacity of non-conventional components

Based on the generic enthalpy model for coal, the special property techniques for enthalpy and density for wood were chosen. The HCOALGEN technique, which is based on ultimate and proximal analysis, was used to compute the OMWS enthalpy. The Kirov correlation uses the proximate analysis to compute the heat capacity of biomass:

$$C_{p,j} = \sum_{j=1}^{ncn} w_j C_{p,ij} \tag{3}$$

where w_j is the mass fraction of the *jth* constituent on a dry basis, *Cp* is the heat capacity, *i* is the component index, *j* is the constituent index. Each proximate analysis' temperature-dependent heat capacity is taken into consideration using the equation below:

$$C_{p,ij} = a_{ij1} + a_{ij2}T + a_{ij3}T^2 + a_{ij4}T^3 \tag{4}$$

where 'a' is a parameter or element, i is the component index, and n is the constituent index (1 = moisture, 2 = FC, 3 = main VM, 4 = secondary VM, 5 = ash). The heat of combustion is used to calculate the standard heat of formation. The char enthalpy was estimated using the identical enthalpy and density procedures as for biomass, with the difference that instead of a manual specification, the heat of combustion was computed using the Boie correlation (5):

$$\Delta_{C2}h_i^{dm} = \left[a_{1i}w_{C,i} + a_{2i}w_{H,i} + a_{3i}w_{S,i} + a_{4i}w_{O,i} + a_{5i}w_{N,i}\right]10^2 + a_{6i} \tag{5}$$

where *w* is the mass fraction of components *C* (carbon), *H* (hydrogen), *S* (sulfur), *O* (oxygen), and *N* (nitrogen). For parameters 1–6, default settings were utilized, which may be found in the Aspen Plus user manuals.

2.2.3- Physical property method

In order to get results that are as accurate and realistic as feasible, modeling procedures necessitate a careful selection of thermodynamic property method. As a result, choosing a property approach was one of the most important aspects of this research. A simulation engine's physical property methods are routines and equations for computing the thermodynamic and transport characteristics of material flows. The simulation can use physical property algorithms to interpret component behavior under various scenarios. Property methods are determined depending on the simulated circumstances and components. Because of the existence of hydrocarbons and light gases, the *RK-SOAVE* property method is used as the global thermodynamic model [36]. *RK-SOAVE* is comparable with *PENG-ROB* but it already contains a number of binary parameters for vapor-liquid and liquid-liquid equilibrium while *PENG-ROB* lacks these parameters. Thermal properties such as enthalpy, density and specific heat are determined from built-in models *HCOALGEN* and *DCHARIGT* in Aspen Plus. The enthalpy of non-conventional component is calculated as

$$H^s = \Delta_f h^s + \int_{T^{ref}}^{T} C_p^s dT \tag{6}$$

As molecular formula of the non-conventional component is unknown so $\Delta_f h^s$cannot be calculated directly. It is possible to calculate heat of formation from heat of combustion as combustion products and their molecular structures are well-known:

$$\Delta_f h^s = \Delta_c h^s + \Delta_f h_{cp}^s \tag{7}$$

$\Delta_f h_{cp}^s$ is the sum of the heats of formation of the combustion products multiplied by the mass fractions of the respective elements in the non-conventional component. Coal enthalpy model

HCOALGEN employs this approach to calculate the enthalpy of non-conventional components. *DCHARIGT* model is based on equations from IGT [41] and calculates density of char on dry basis using ultimate and sulfur analyses. As both conventional and non-conventional solids are involved in the simulation model, stream class *MCINCPSD* is a suitable choice. Molecular weights and other thermos-physical properties are retrieved from NIST database.

Aspen plus is flexible enough to integrate other programs like Fortran user-subroutines or Matlab. This feature is intended to model highly complex reactor models which otherwise cannot be used in predefined blocks in Aspen Plus.

The kinetic reactions of pyrolysis are written in a separate Fortran file and then compiled using an intel compiler. The external Fortran user-subroutine is then coupled with Aspen Plus using a *dll* file. This method of coupling is different from the Fortran calculator blocks already embedded in Aspen Plus. Reactor inputs e.g. mass flow rate, temperature, volume etc. are transferred to Fortran file where chemical reactions take place by using empirical correlations and products are formed as a function of temperature. The results are sent back to Aspen Plus and can be seen in the output tab of the reactor.

2.2.4- Pyrolysis section

For present study, fluidized bed reactor is 500 mm long and 50 mm in diameter with 100 µm orifice diameter of gas distributor. 160 grams of OMWS, 40 grams of biochar, 5 l/min of carrier gas (Nitrogen) and 13.3 l/min of fluidization gas (Nitrogen) are fed into the reactor. The residence time of the vapors is 2 seconds.

Two Aspen plus unit operations, the fluidized bed reactor (FBR) and pyrolysis reactor (*RCSTR*) are used to represent the pyrolysis section. The fluidized bed mimics the fluidization model of solids and calculates the minimum fluidization velocity. The *RCSTR* reactor represents the pyrolysis reactor where biomass is converted into pyrolysis products. Template

for reaction kinetics is unable to deal with the kinetics of equations (8) and (9), so kinetic equations for OMWS pyrolysis are written in an external Fortran user-subroutine and then linked with *RCSTR* reactor (Figure 4). A general reaction is given by equation (2).

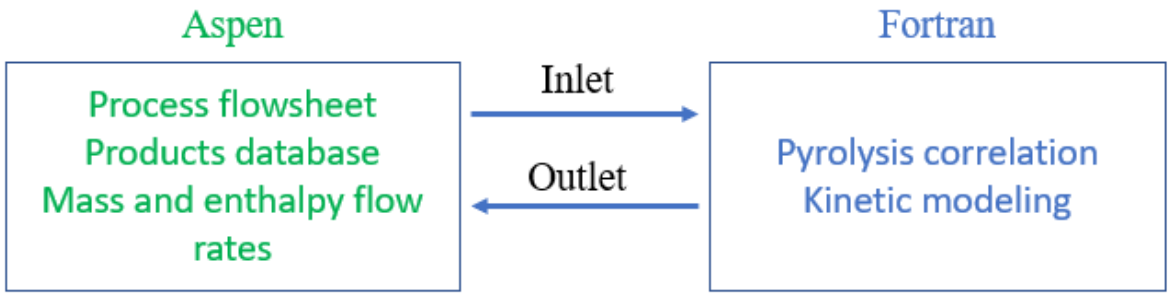

Figure 4. Coupling of external user-subroutine with Aspen plus.

The reaction rate of the pyrolysis of OMWS is determined from the analysis of experimental data of Agblevor et. al. [35] and formulated according to the modified Arrhenus law proposed by Diaz and Broun [42].

$$R = k.C_{ko}.(\frac{F_k}{F_{ko}})^n \quad (8)$$

where R, k,, C_{ko}, F_k, F_{ko} and n are reaction rate (kg/m^3.s), rate constant (1/s), concentration of OMWS (kg/m^3), remaining mass flow (kg/s), initial mass flow of OMWS (kg/s) and Order of reaction (n=1) respectively. The rate constant can be written by the following equation:

$$k = A\,exp\left(\frac{E_a}{RT}\right) \quad (9)$$

where A is pre-exponentiel factor (A= 2.55×10^4 s^{-1}), E_a is Activation Energy (E_a = 69.56 kJ/mol/K), T is temperature (K) and R is gas constant (J/mol. K). The subsequent production of bio-oil, biochar, NCG and water is calculated by the following relation [42,43] .

$$R_i = f_i \times R \quad (10)$$

where:

R_i = reaction rate of i-th product, kg of i-th product/m^3.s

f_i = stoichiometric factor of i-th product, kg of i-th product/kg of OMWS

286 f_i used in this model is based on the experimental data at 400°C, 450°C and 500°C and given
287 in the following Table 4.

288 **Table 4.** f_i determined from experimental data of Agblevor et al. [8] and used in the model.

Component	f_i (kg/kg of OMWS) 400°C	f_i (kg/kg of OMWS) 450°C	f_i (kg/kg of OMWS) 500°C
CHAR	0.291	0.227	0.204
H_2O	0.113	0.175	0.118
H_2	0.005375	0.0114	0.01486
CO	0.01485	0.02205	0.045003
CO_2	0.196	0.21765	0.252972
CH_4	0.004	0.0078	0.014554
C_2H_6	0.0125	0.0162	0.02267
C_3H_8	0.0125	0.0162	0.02298
C_4H_{10}	0.00475	0.0.0087	0.009958
Bio-oil	0.346	0.298	0.295

289

290 *2.2.5- Condensers*

291 Shell and tube heat exchangers were used to model the condensers in Aspen Plus. The
292 diameter of the shell is 60 mm and tube length is 500 mm with 20 mm diameter (Figure 2).
293 Water/ethylene glycol mixture is used as cooling medium at 8°C with flow rate of 8 kg/hr in
294 each heat exchanger. The components used in the simulation model are summarized in Table
295 5.

296 **Table 5.** List of components

Component ID	Type	Component Name	Alias
OMWS	Nonconventional		
CHAR	Nonconventional		
Ash	Nonconventional		
N_2	Conventional	NITROGEN	N_2
O_2	Conventional	OXYGEN	O_2
H_2	Conventional	HYDROGEN	H_2

H_2O	Conventional	WATER	H_2O
CO	Conventional	CARBON-MONOXIDE	CO
CO_2	Conventional	CARBON-DIOXIDE	CO_2
CH_4	Conventional	METHANE	CH_4
C_2H_6	Conventional	ETHANE	C_2H_6
C_3H_8	Conventional	PROPANE	C_3H_8
C_4H_{10}	Conventional	ISOBUTANE	C_4H_{10}-2
Fe_2O_3	Solid	HEMATITE	Fe_2O_3
Al_2O_3	Solid	ALUMINIUM-OXIDE-ALPHA-CORUNDUM	Al_2O_3
SiO_2	Solid	SILICON-DIOXIDE	SiO_2
TiO_2	Solid	TITANIUM-DIOXIDE-RUTILE	TiO_2
Na_2O	Solid	SODIUM-OXIDE	Na_2O
CaO	Solid	CALCIUM-OXIDE	CaO
ETHYL-01	Conventional	ETHYLENE-GLYCOL	$C_2H_6O_2$
R22	Conventional	CHLORODIFLUOROMETHANE	$CHClF_2$
Catalytic Bio-oil			
1-DECENE	Conventional	1-DECENE	$C_{10}H_{20}$-5
P-CRESOL	Conventional	P-CRESOL	C_7H_8O-5
1-UNDECE	Conventional	1-UNDECENE	$C_{11}H_{22}$-2
N-UNDECA	Conventional	N-UNDECANE	$C_{11}H_{24}$
4-ETHPHE	Conventional	P-ETHYLPHENOL	$C_8H_{10}O$-3
2-DODECA	Conventional	DECYL-METHYL-KETONE	$C_{12}H_{24}O$-N9
1-TRIDEC	Conventional	1-TRIDECENE	$C_{13}H_{26}$-2
N-TRIDEC	Conventional	1-TRIDECANOL	$C_{13}H_{28}O$
HEXADECA	Conventional	N-HEXADECANE	$C_{16}H_{34}$
1-TETRAD	Conventional	1-TETRADECENE	$C_{14}H_{28}$-2
TETRADEC	Conventional	N-TETRADECANE	$C_{14}H_{30}$
N-PENTAD	Conventional	1-PENTADECANOL	$C_{15}H_{32}O$
HEPTADEC	Conventional	N-HEPTADECANE	$C_{17}H_{36}$
1-HEPTAD	Conventional	1-HEPTADECENE	$C_{17}H_{34}$-D1
1-NON-DE	Conventional	1-NONADECANOL	$C_{19}H_{40}O$
PALMI-01	Conventional	PALMITONITRILE	$C_{16}H_{31}N$
TRICY-01	Conventional	TRICYCLOHEXYLAMINE	$C_{18}H_{33}N$
ETHYL-01	Conventional	ETHYL-OLEATE	$C_{20}H_{38}O_2$-N1
BUTYL-01	Conventional	BUTYL-OLEATE	$C_{22}H_{42}O_2$-N5
9-HEP-01	Conventional	9-HEPTADECANONE	$C_{17}H_{34}O$
Non-Catalytic bio-oil			
N-PEN-01	Conventional	N-PENTADECANE	$C_{15}H_{32}$
8-HEP-01	Conventional	8-HEPTADECENE	$C_{17}H_{34}$-N4
1-HEP-01	Conventional	1-HEPTADECENE	$C_{17}H_{34}$-D1
N-HEP-01	Conventional	N-HEPTADECANE	$C_{17}H_{36}$
N-HEX-01	Conventional	N-HEXADECANOIC-ACID	$C_{16}H_{32}O_2$
METHY-01	Conventional	METHYL-PALMITATE	$C_{17}H_{34}O_2$-N1
METHY-02	Conventional	METHYL-OLEATE	$C_{19}H_{36}O_2$
OLEIC-01	Conventional	OLEIC-ACID	$C_{18}H_{34}O_2$

297

298 *2.3- Industrial scale*

299 A simulation model of a hypothetical plant of 100 tonnes/day wet OMWS (93 tonnes/day
300 dry OMWS) capacity is developed. The overall technique used in this analysis is depicted in
301 Figure 5. Modeling, equipment size and costing, profitability analysis using the discounted
302 cash flow (DCF) approach, and sensitivity analysis are all part of the methodology.

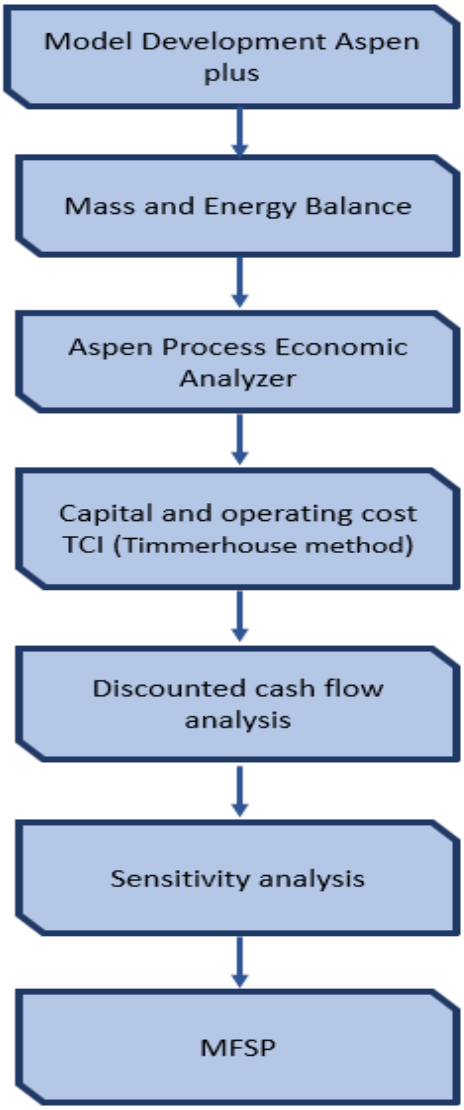

303

304 **Figure 5**. Methodology flow chart

Process overview can be seen in Figure 6. It is divided into seven major technical parts: (i) Preprocessing of feedstock (Area 100); (ii) Bio-oil production via catalytic fast pyrolysis (Area 200); (iii) Solids removal (Area 400); (iv) Bio-oil condensation (Area 400); (v) Compression/absorption machine (Area 500); (vi) Heat generation (Area 600); (vii) Electricity generation (Area 700).

In the feed processing section (Area 100), wet biomass is ground to less than 2 mm and then dried to reduce the moisture from 20% to 4% to meet the feed requirements of pyrolysis reactor. Pyrolysis takes place in Area 200 where OMWS is converted to bio-oil, biochar and non-condensable gases (NCG). The pyrolysis products are then fed into solids removal section (Area 300), which separates the solid particles (catalyst and biochar) from the hot bio-oil vapors and gases. The condensation of bio-oil vapors is achieved in the liquid recovery section (Area 400), using a compression refrigeration machine or an absorption refrigeration machine (Area 500). The biochar separated from bio-oil vapors is combusted in heat generation section (Area 600) to regenerate catalyst and produce heat (flue gases) to be used for drying of wet biomass and fast pyrolysis process.

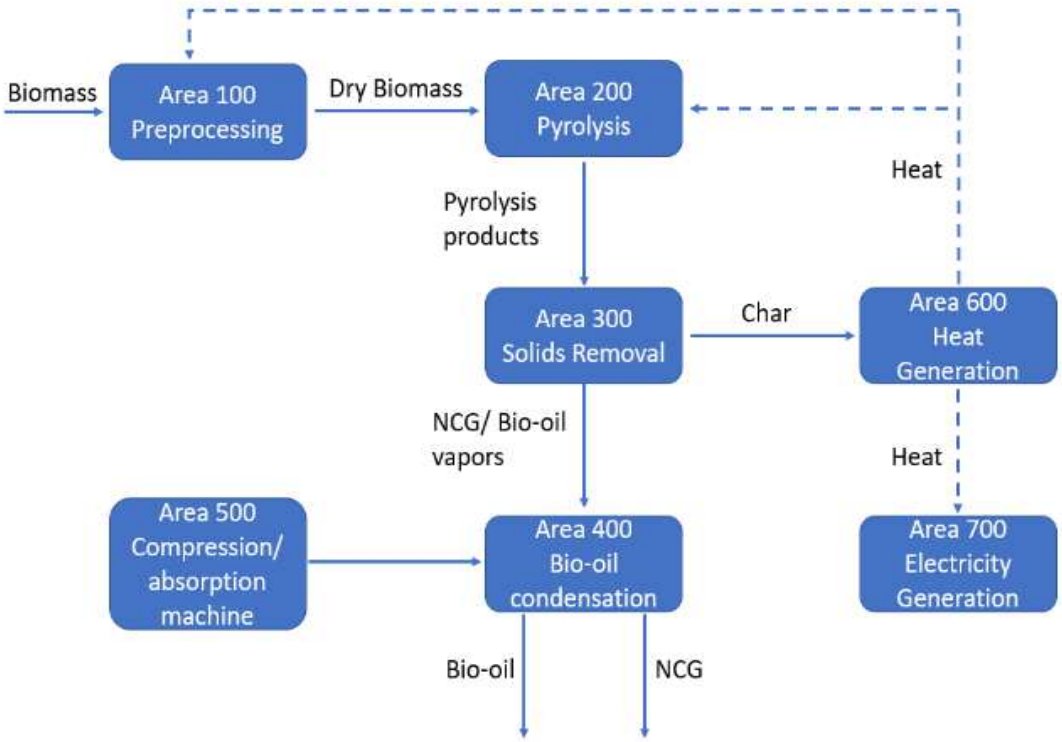

Figure 6. Process overview

2.3.1- Model Development

The model is divided into different subsections (Area 100 - Area 700) for better elaboration. Aspen Plus flowsheet can be seen in Figures 9 and 10. A heat exchangers network is presented in Figure 11. HX-1 and HX-2 are the first and second condensers, HX-3 is for heating the fluidizing gas, HX-4 is employed for steam production and HX-5 is used to heat the air for biomass drying.

2.3.1.1- Feedstock preparation (Area 100)

Olive mill wastewater sludge (OMWS) collected from Sfax, Tunisia with an initial size of 200 mm is supplied to two hammer mills separated by a screen for particle separation. The biomass is ground to 2 mm as required by pyrolysis reactor. The exiting wet biomass with initial moisture content of 20% is dried in a convective dryer at an operating temperature of 120°C to reduce the moisture content to 4%. The heat for drying purpose is supplied by flue gases coming from combustion of biochar (Area 600). The dried biomass is mixed with 20% of

335 biochar to make it less sticky and fed into the pyrolysis reactor smoothly. Table 1 summarizes
336 properties of OMWS [35].

337 *2.3.1.2- Pyrolysis (Area 200)*

338 In the pyrolysis section, pre-treated biomass is converted into bio-oil vapors, biochar,
339 and non-condensable gases (NCG) in two virtual stages as discussed in section 3.2.1. The
340 pyrolysis reaction was modelled using kinetic parameters derived from Agblevor et. al. [35]
341 experimental findings. High-efficiency cyclones separate biochar from a mixture of gas and
342 vapors, which is then fed into a combustor.

343 The heat required for the pyrolysis reaction is provided by char combustion in Area
344 600. The residual heat is used to dry wet biomass and to produce superheated steam, which is
345 then extended to generate 0.6 MW of electricity. The pyrolysis product mass flow rates are
346 given in Table 12.

347 *2.3.1.3- Solids Removal Area (Area 300)*

348 In Area 300, a high-performance cyclone separates the entrained catalyst fines and
349 biochar from the gases and vapors, achieving a separation efficiency of 0.9. To completely
350 remove the biochar and catalyst particulates from the products, another hot gas filter is
351 employed.

352 *2.3.1.4- Bio-oil condensation (Area 400)*

353 The hot product gases pass through the first condenser at 400°C and leave the first
354 condenser at around 100°C condensing about 70% of bio-oil. About 685 kW of heat is removed
355 in the first condenser. The cooled products are sent to another condenser where they are cooled
356 to around 40°C and remaining bio-oil and water are condensed. In the second condenser, 237
357 kW of heat is removed. The remaining fraction of bio-oil vapors is passed through an
358 electrostatic precipitator to quench the bio-oil.

2.3.1.5- Refrigeration machine (Area 500)

Two cooling machines were modelled in this study: (i) Vapor compression refrigeration machine (scheme-1) (ii) absorption refrigeration machine (LiBr-H_2O) (scheme-2). In scheme-1, a conventional vapor compression refrigeration system is developed. The system is modelled with a compressor, condenser, valve and a heat exchanger (evaporator). Total cooling load required for both condensers is 922 kW. The refrigerant employed in the simulation for the refrigeration is R-22 and *REFPROP* is used as base method. Annually 5.4 million kWh of energy is removed in the first condenser and 1.8 million kWh in the second condenser.

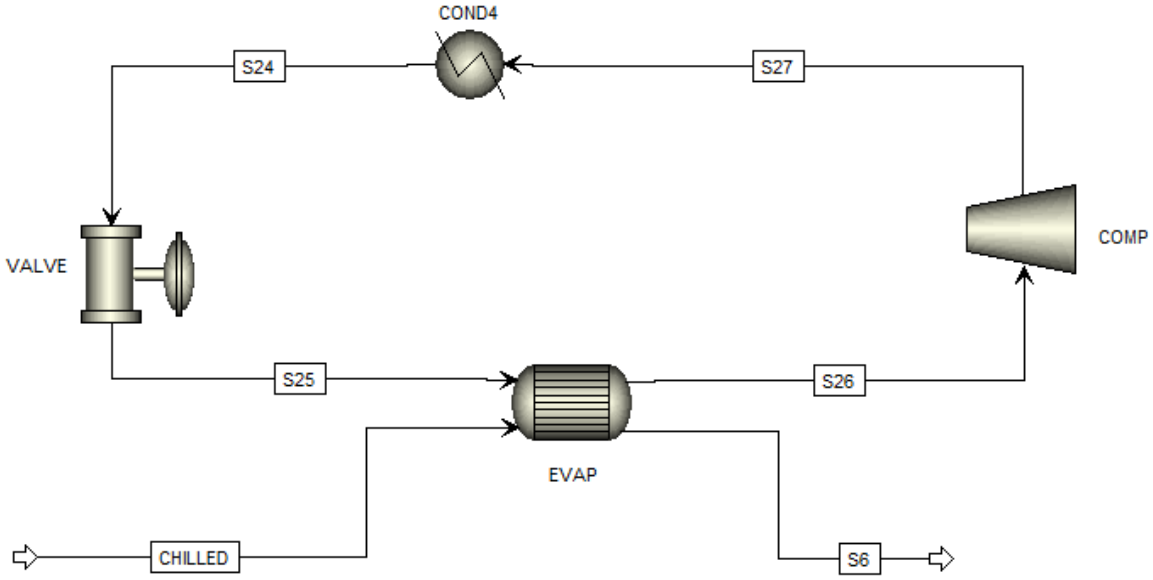

Figure 7. Compression refrigeration machine

In scheme-2, the absorption refrigeration machine operates by recovering heat from the first condenser. The absorption machine is modelled for a cooling capacity of 237 kW. The cooling produced is used to cool down the pyrolysis products in the second condenser. The absorption system is modelled on the work of Somers et. al. [44]. Because the operating parameters and fluids being modeled with this approach are designed for electrolytes, the activity coefficient property method in ASPEN (*ELECNRTL*) is used for the water/LiBr solution. [45]. The *steamNBS* tables were utilized for the pure water states [46].

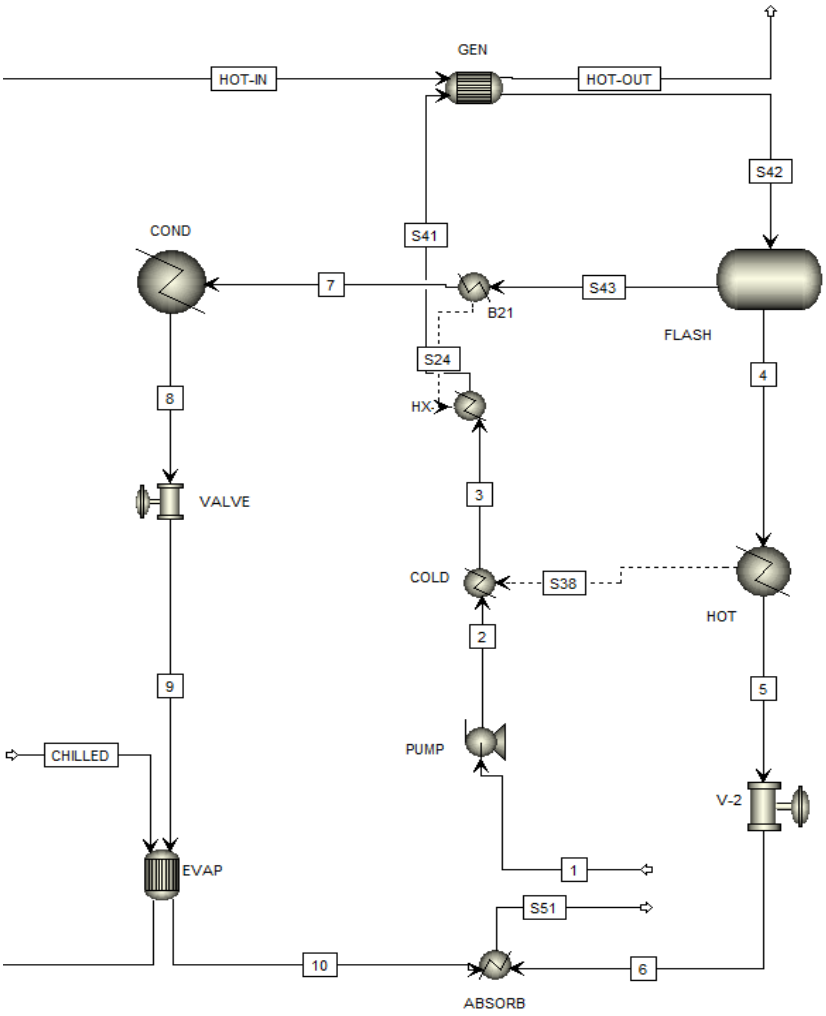

Figure 8. Absorption refrigeration machine

2.3.1.6- Catalyst Regeneration (Area 600)

The biochar is treated as a non-conventional component in this model, so the ultimate analysis of the biochar needs to be determined as well. The ultimate analysis of biochar is computed by the elemental balance in OMWS, gaseous components from OMWS pyrolysis and biochar. A general formula to calculate the percentage of carbon in biochar is given by

$$C_{biochar}\% = \frac{C_{OMWS}\% - \left(\frac{f_{CO}}{28} + \frac{f_{CO_2}}{44} + \frac{f_{CH_4}}{16} + \frac{f_{C_2H_6}}{30} \times 2 + \frac{f_{C_3H_8}}{44} \times 3 + \frac{f_{C_4H_{10}}}{58} \times 4 + \frac{f_{Biooil}}{MW_{biooil}} \times N_{Biooil}\right)}{f_{Biochar}} \quad (11)$$

The percentages of other elements are calculated in the same manner.

The combustion of biochar is given by following reaction

$$Biochar + O_2 = CO_2 + H_2O + NO_2 + SO_2 \quad (12)$$

385 Biochar and catalyst exiting the cyclone are combusted in a combustor (*RStoic*). The
386 biochar is combusted with excess air at a temperature of 1400°C. The heat generated is used to
387 heat the pyrolysis reactor reducing the temperature of exhaust gases to 1000°C. In Area 700,
388 these gases are utilized to produce superheated steam, which is then used to generate power.
389 Finally, after steam generation, the exhaust gases are still hot to be used in drying the wet
390 biomass in Area 100.

391 *2.3.1.7- Electricity generation (Area 700)*

392 The heat generated by combustion of biochar in Area 600 is used to produce steam,
393 which is then used to generate electricity. The steam power cycle was modelled using a steam
394 turbine, a heat exchanger, a condenser, and a feed water pump. The *NBS/NRC* steam table in
395 Aspen Plus was employed to model the thermodynamic properties of the water portion of the
396 heat exchanger. Superheated steam was produced at 503°C and fed into the steam turbine to
397 generate electricity. The steam turbine was specified at 95% mechanical efficiency and 80%
398 isentropic [32].

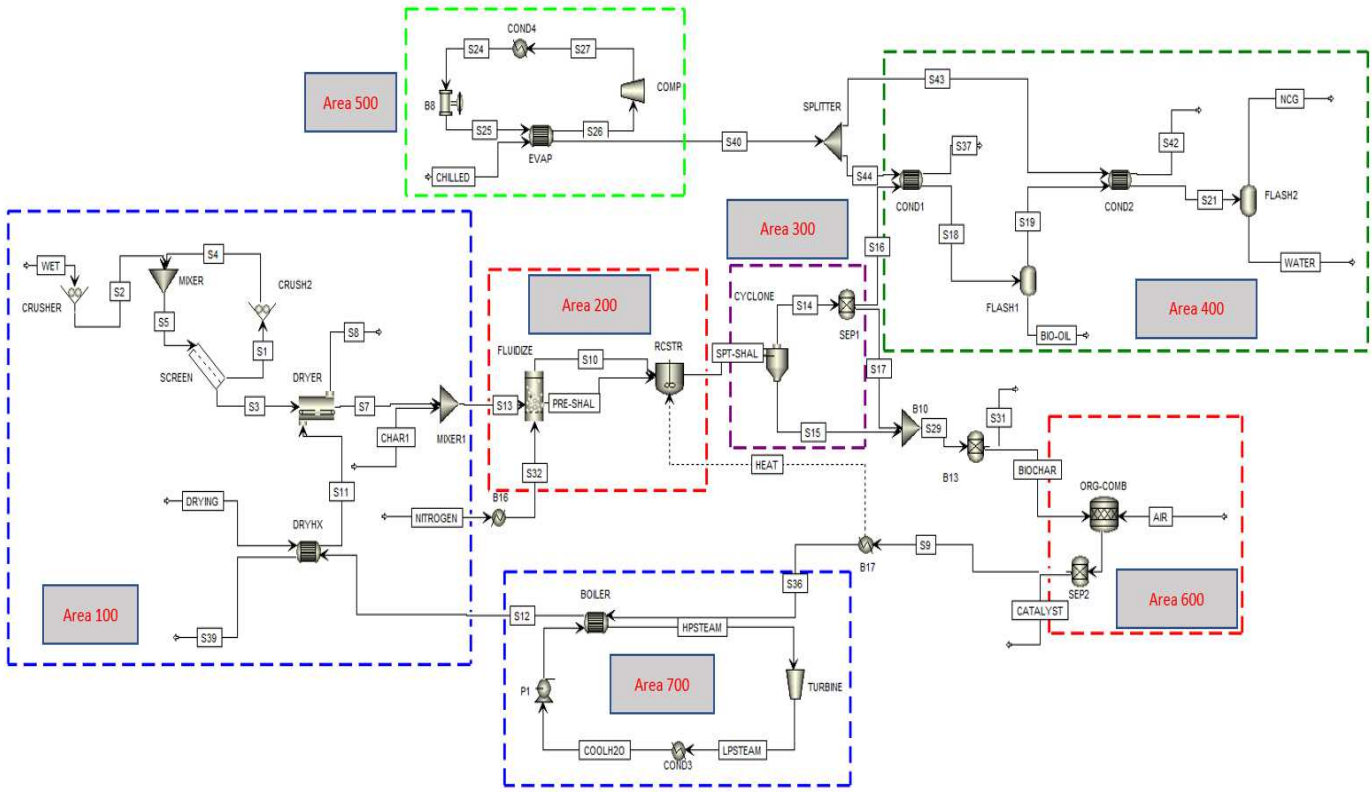

399

400 **Figure 9.** Process flow diagram with compression refrigeration machine

401

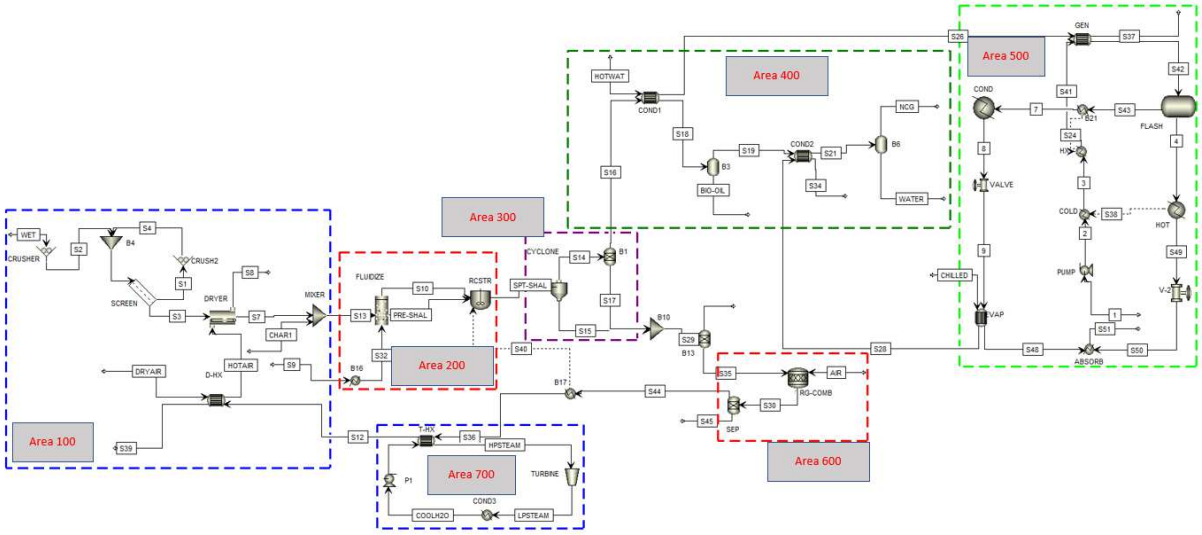

402

403 **Figure 10.** Process flow diagram with absorption refrigeration machine

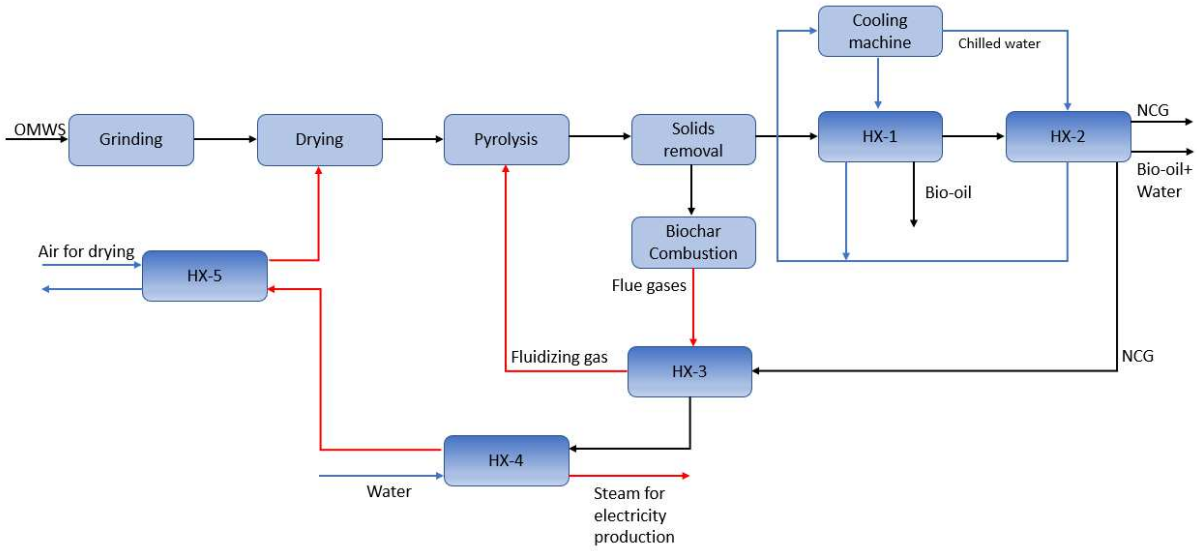

Figure 11. Heat exchangers network

2.4- Performance parameters

Energy efficiency of the system is calculated by dividing energy output from the system by the energy input to the system. The energy efficiency formula is shown in eq. 13 [32].

$$\eta_{plant} = \frac{\dot{m}_o . LHV_o + W_o}{\sum_i (\dot{m}_i . LHV_i) + \sum W_i + Q_i} \quad (13)$$

where $\dot{m}_o$ represents the mass flow rate of bio-oil and gaseous products and LHV_o represents the corresponding lower heating value. W_o represents the electricity generated by the turbine. Similarly, $\dot{m}_i$ and LHV_i are the biomass flow rate and lower heating value respectively. W_i is total power required to operate the complete system including pumps, dryer, grinder, compressor and cyclones. Th hot utility utilized in the plant is represented by Q_i.

Absolute average deviation e between simulated and experimental results is given by [47]:

$$e\ (\%) = 100 \times \left(\sum_i^N \frac{|Y_{i,sim} - Y_{i,exp}|}{Y_{i,exp}} \right) \Big/ N \quad (14)$$

where $Y_{i,sim}$ is the quantity of a product calculated by simulation model and $Y_{i,exp}$ is the experimental quantity of a product.

417 *2.4.1- Process Economics*

418 *2.4.1.1- Cost Estimation*

419 Aspen Process Economic Analyzer (APEA) was used to size equipment and estimate
420 costs. To conduct sizing measurements and approximate equipment procurement costs, the unit
421 operations modelled in Aspen Plus are sent to APEA where they are mapped and sized to the
422 desired equipment cost models. The costs of pyrolysis reactor and regenerator were calculated
423 using scaling equation as stated by Wright et al. [33].

$$C_1 = C_o.\left(\frac{S_1}{S_o}\right)^{0.6} \quad (15)$$

424 where C_1 is the new calculated cost with the size of S_1 and C_o is the base cost with the size of
425 S_o. The equipment cost is updated to current year (2021) by using the Chemical Engineering
426 Plant Cost Index (CEPCI) by employing the following equation [9].

$$New\ equipment\ cost = Base\ equipment\ cost \times \frac{2021\ cost\ index\ value}{Base\ year\ cost\ index\ value} \quad (16)$$

427 CEPCI for 2021 is listed as 754.7 and for 2018 is 603.1 [48].

428 Table 6 shows the assumptions made during the calculation of total operating cost.

429 **Table 6.** Operating cost parameters

Material	**Cost**
Biomass cost [€/t]	30
Catalyst [€/kg]	3
Utilities	
Electricity [€/kWh] [49]	0.065
Cooling water [€/m^3]	0.032

430

431 The project will be based in Tunisia, and new tax legislation has been enacted as a result of
432 the devastating economic impact of Covid-19 on the nation. According to the 2021 Finance

433 Law, a corporate income tax rate of 10% applies to investments in agriculture, fisheries,
434 handicrafts, pollution control, and so on, while a rate of 35% applies to the financial sector,
435 oil and gas, telecommunications etc. [50].

436 **Table 7.** Inputs for DCF analysis

Economic Inputs	
Required rate of return	10%
Plant life	20 years
Capital cost escalation	5%
Revenue escalation	5%
Operating cost escalation	3%
Income Tax	40%

437

438 **Table 8.** Variation in different parameters

Parameter	**Range**
Fuel yield [kg/year]	± 30%
Capital cost [€]	± 30%
Operating cost [€]	± 30%
Income tax [%]	10% to 60%
Discount rate [%]	0% to 40%

439

440 Total project investment was calculated using Peters and Timmerhaus's method [51] as
441 shown in Table 9. The capital cost of the pyrolysis plant is made up of direct and indirect costs,
442 as well as a contingency and location factor. Regional labor, supervisor, and service costs are
443 included in the cost model. Total installed cost (TIC) is approximated by 3.02 times the
444 purchased cost of equipment. Installation cost includes electrical wiring, plumbing, structures,

and other related costs. Indirect costs include contractor's fees, supervision and technical cost, legal fees and construction costs. It is calculated at a rate of 0.89 times the total purchased equipment cost.

Table 9. Total project investment estimation method [20,51]

Parameter	Value
Total purchase equipment cost (TPEC)	100% TPEC
Total installed cost (TIC)	302% TPEC
Indirect cost (IC)	89% TPEC
Total direct and indirect cost (TDIC)	TIC + IC
Contingency	20% TDIC
Fixed capital investment (FCI)	TDIC + contingency
Location factor (LF)	10% FCI
Total project investment (TPI)	FCI + LF

2.4.1.2- Profitability analysis

The discounted cash flow approach was used to assess the profitability of all process schemes. The minimum fuel selling price (MFSP) is calculated by setting the NPV to zero in equation 17.

$$NPV = -C_T + \sum_{n=1}^{N=t} \frac{\emptyset\, \dot{m}(1 - T_n) - O_n}{(1 + r)^n} \quad (17)$$

where C_T represents the initial capital investment, $\emptyset$ is the fuel price, annual fuel yield of plant is specified by $\dot{m}$, annual operating cost is represented by O_n, T_n is annual income tax and r is the required rate of return. The plant is assumed to be operational for a 20-year period (t) in the DCF analysis.

458 *2.4.1.3- Sensitivity Analysis*

459 Sensitivity analysis is a method for assessing the profitability effect of improvements
460 in procedure and economic parameters. The effect of key parameters on the MFSP, such as
461 bio-oil yield, capital investment, operational cost, discounted rate and income tax was
462 investigated. These parameters were selected because they have a clear connection to
463 profitability; in other words, the MFSP of bio-oil is closely related to these parameters. A
464 30% spectrum is used in the sensitivity analysis. Although the specified spectrum of the
465 sensitivity analysis allows for individual evaluation of uncertainty in parameter estimates, it
466 does so in a deterministic fashion that ignores the studied parameters.

467 ## 3- Results and discussions

468 *3.1- Model Validation*

469 Simulations were performed in Aspen Plus based on fluidized bed data for non-
470 catalytic and catalytic fast pyrolysis processes. To determine the accuracy of the developed
471 fluidized bed fast pyrolysis model, bio-oil, bio-char, and NCG yields were compared with the
472 experimental results reported by the work of Agblevor et al. [35]. The fast pyrolysis process
473 with and without catalyst was simulated under identical conditions in experimental studies of
474 Agblevor et. al. [35] by using input and output variables such as reactor temperature,
475 characteristics of biomass, catalyst, and the flow rate of feedstock, etc.

476 *3.1.1- Non-Catalytic fast pyrolysis*

477 After defining the proximate, ultimate and chemical analyses of each component used
478 in the proposed model, the simulation was performed at different pyrolysis temperatures 400,
479 450 and 500°C using Aspen Plus to compute the yields of the different products; bio-oil,
480 biochar, NCG and water. The obtained results of the product yields are presented in Figures
481 12, 13 and 14 compared with experimental data. The absolute average deviation (AAD) at

different temperatures is illustrated in Table 10. It depicts the closeness of simulation results to the experimental data.

As shown in Figures 12, 13 and 14, the trend of product yields between simulation results, for non-catalytic fast pyrolysis, satisfactorily represents the experimental data with AAD for bio-oil, biochar, NCG, and water range from 0.53% to 1.95%, 1.52% to 2.91%, 1.96% to 2.70% and 3.39% to 9.77% respectively. In addition, the sensitivity of the product yields on pyrolysis temperature was simulated and investigated. The simulation results depicted in Figures 12-14 show that the yield of bio-oil increases with increasing reaction temperature and reaches a maximum of 36.6 wt.% at a pyrolysis temperature of 450°C. The low bio-oil yield obtained from the fast pyrolysis of OMWS is expected since the composition of the polymers which constitute OMWS is not the same and the properties of OMWS have high ash content which favors charring reaction [52]. Above 450°C, the bio-oil yield decreases slightly with increasing temperature. Therefore, the optimum pyrolysis temperature for bio-oil production from OMWS is 450°C which is low if compared with other lignocellulosic biomasses cited in the literature. This difference is due to the chemical composition of biomass which affects not only the pyrolysis product yield but also pyrolysis temperature.

Table 10. Absolute average deviation (e) for different temperatures

Product	*e* (%) 400°C	*e* (%) 450°C	*e* (%) 500°C
Bio-oil	0.53	1.95	0.99
Biochar	2.91	1.52	1.84
NCG	2.70	2.40	1.96
Water	3.46	3.39	9.77
Overall	2.40	2.32	3.64
Global		2.78%	

Furthermore, the product yields analysis of non-catalytic pyrolysis shows the decrease of biochar and the increase of the gas yield when the pyrolysis temperature increases. This can be explained by the secondary reactions of decomposition of the solid formed during the fast pyrolysis to produce bio-oil and gas. It can be also noted that the increase in the gas yield and decrease in the bio-oil yield above 450°C is due to the secondary cracking reaction occurring in the vapors.

In general, the water is yielded from the pyrolysis process at a temperature below 200°C and is present among the products of OMWS since the water gas shift reaction does not take place in the range temperature between 400 to 500°C. In addition, it can be observed that the yield of pyrolytic water is slightly affected by the pyrolysis temperature.

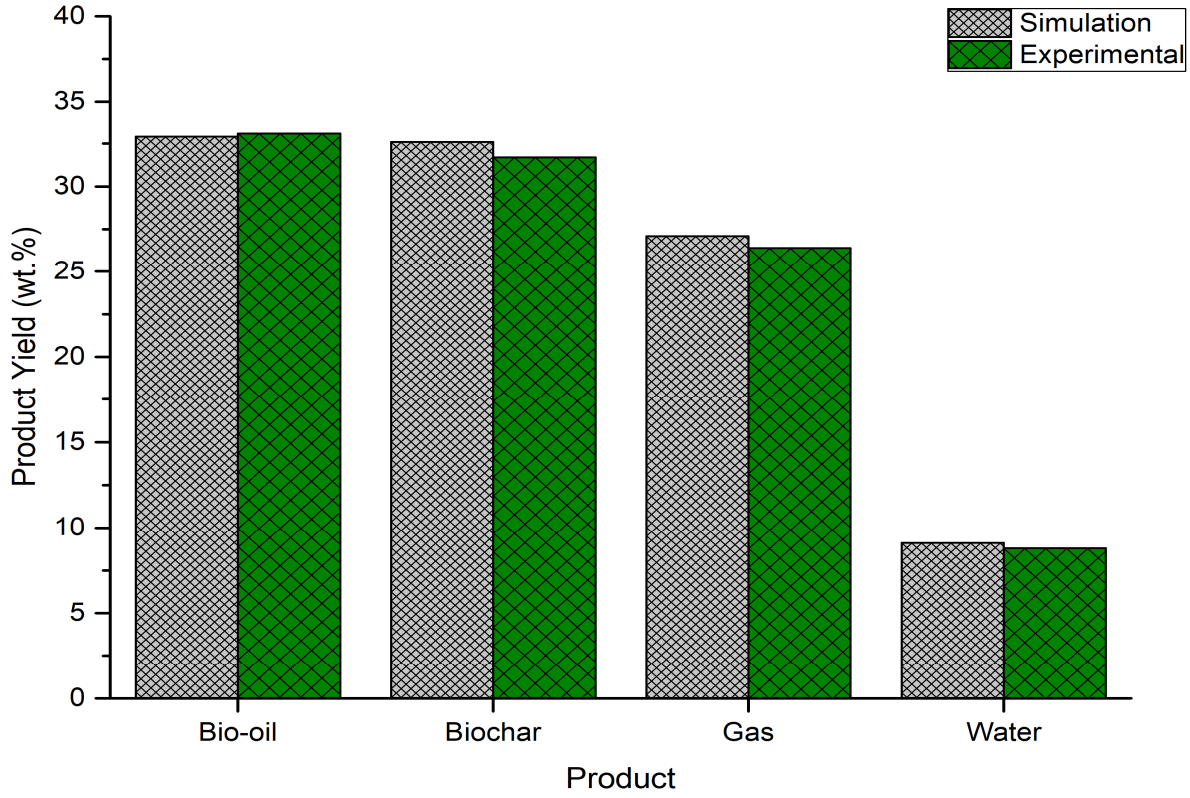

Figure 12. Comparison between simulation and experimental yields at 400°C

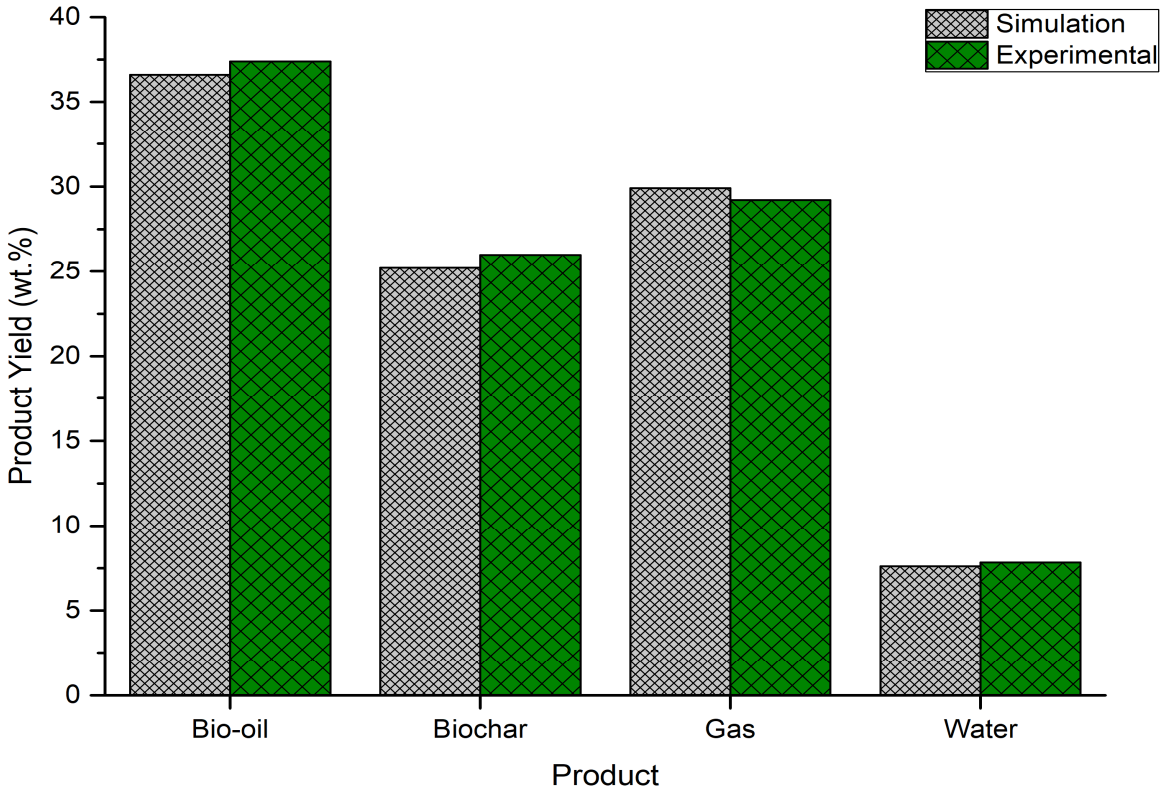

514

515 **Figure 13.** Comparison between simulation and experimental yields at 450°C

516

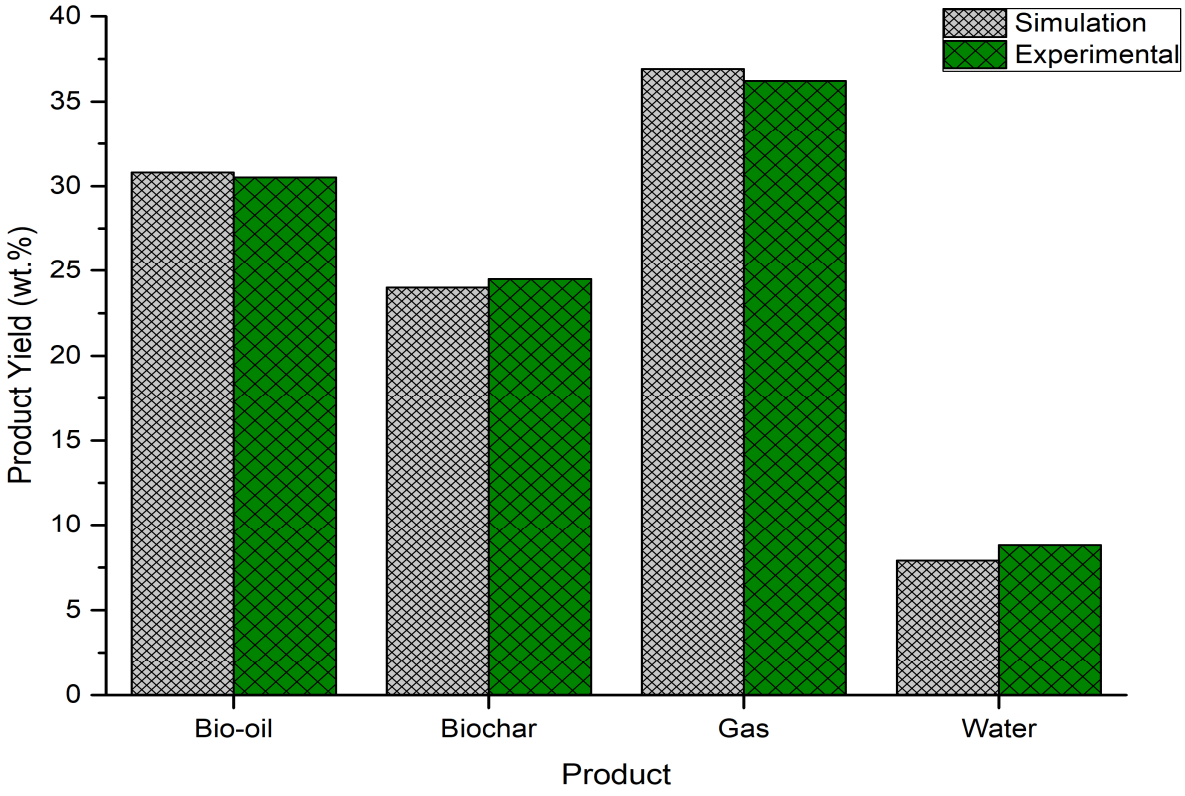

517

518 **Figure 14.** Comparison between simulation and experimental yields at 500°C

519 The effect of pyrolysis temperature on the gas composition was also simulated and
520 was depicted in the Figure 15 with the experimental results. Model simulations in the range of
521 pyrolysis temperature between 400 to 500°C show that the product gases distribution of the
522 non-catalytic fast pyrolysis of OMWS contains the notable gas species: carbon dioxide (CO_2),
523 carbon monoxide (CO), ethane (C_2H_6), propane (C_3H_8), butane (C_4H_{10}) and methane (CH_4)
524 but hydrogen (H_2) is found in trace amounts. The deviations of the model predictions from the
525 experiments are less noticeable for all gas species at different pyrolysis temperatures.
526 Figure 15a shows that CO_2 represents 81.09 wt.% of total gases at temperature 400 °C thanks
527 to the fatty acids compounds present in the OMWS and the gases CO and CH_4 represent
528 4.71% and 1.50% respectively because their production is carried out at higher temperature.
529 The presence of CH_4 within the composition of gases is useful and interesting as a source of
530 fuel.
531 As shown in Fig. 15a-c, CO_2 yield decreased and the yield of CO, CH_4, C_2H_6, C_3H_8
532 and C_4H_{10} slightly increased when the temperature increased. The diminution of the CO_2 is
533 due to its decomposition to generate more CO. This result is reported Paviet et. al. [53] who
534 studied the effect of temperature parameter on the thermochemical treatment of biomass. No
535 significant effect is observed by the increase of the temperature on H_2 gas.
536

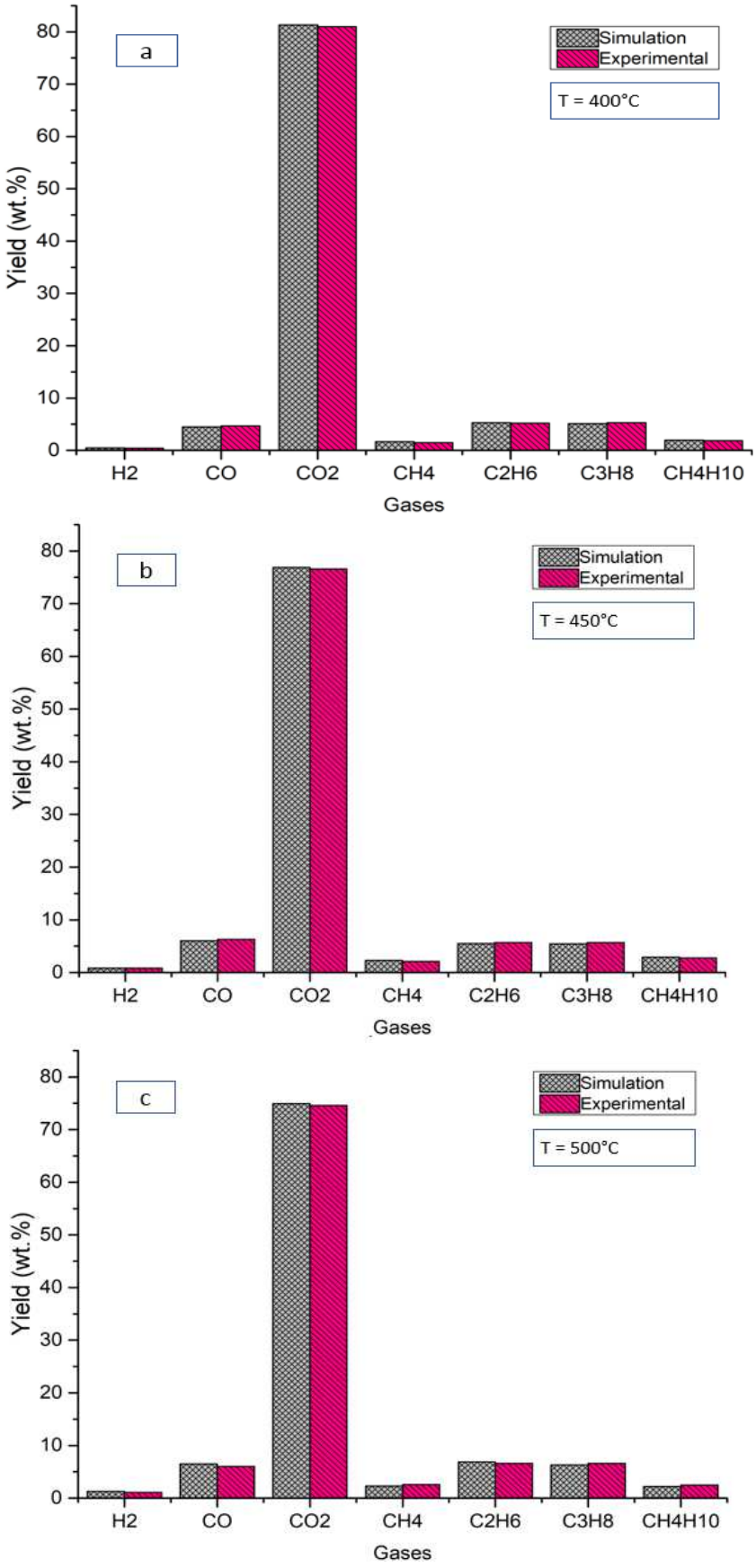

Figure 15. Distribution of gas composition during non-catalytic fast pyrolysis.

In order to demonstrate how the Aspen model performs in predicting individual bio-oil compounds for non-catalytic fast pyrolysis, model predictions at 450°C were compared with experimental data as shown in Figure 16. It can be seen that the simulation results have similar experimental results for the bio-oil composition. In addition, by comparing the experimental data and simulation results for the yield of each compound of the bio-oil, it can be noted that the higher composition of each individual compound in the simulation model is due to the fact that it was not possible to determine the identity of some compounds experimentally. Subsequently, the model takes into account these compounds as unknown compounds and to accommodate these unknown compounds, the weight percentage of known compounds was higher in the simulation model.

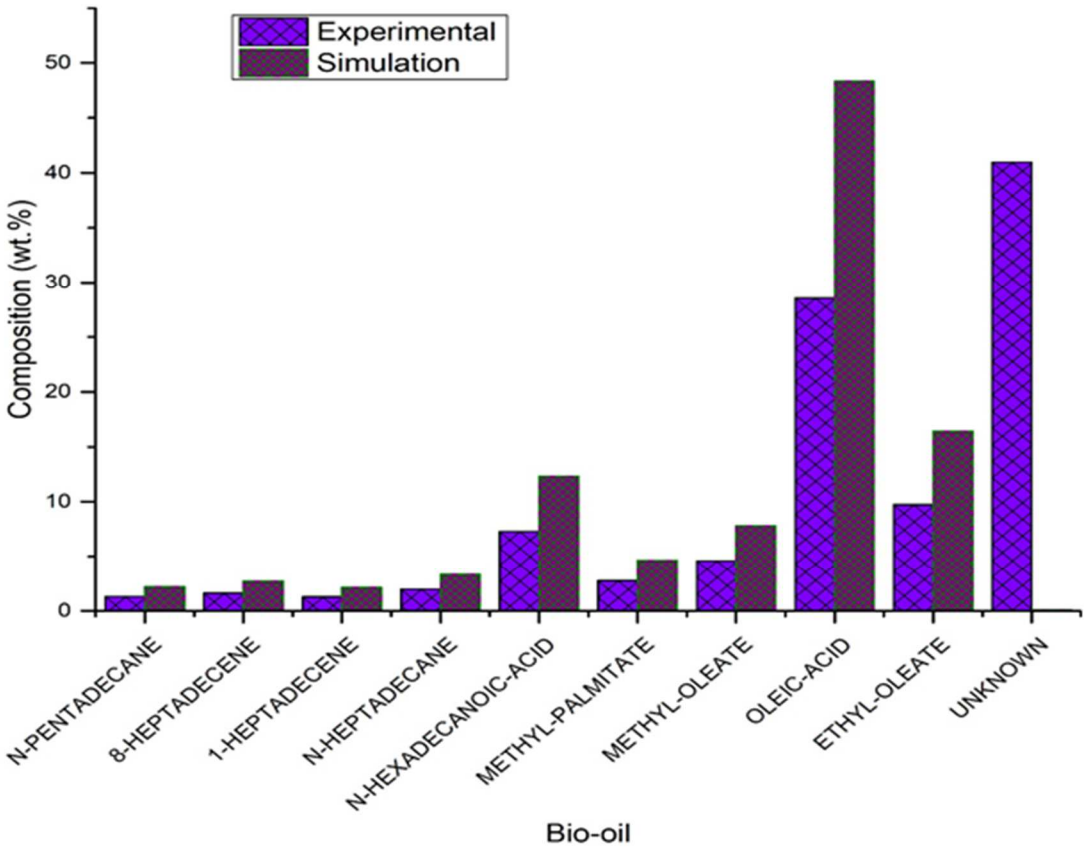

Figure 16. Bio-oil composition at 450 °C for non-catalytic fast pyrolysis.

3.1.2- Catalytic fast pyrolysis

The non-catalytic fast pyrolysis results of OMWS investigated by Agblevor et. al. [35] showed that the pyrolytic OMWS bio-oil had high oxygen content and viscosity. To upgrade the quality of this bio-oil, Agblevor et. al. [35] investigated in situ catalytic fast pyrolysis process using red med as a catalyst. In this case, the Aspen Plus model was also developed to simulate the catalytic fast pyrolysis of OMWS at the same temperature used in non-catalytic pyrolysis. The model was validated against the experiments of Agblevor et. al. [35] conducted in a fluidized bed pyrolyzer. The simulation results with experimental data of the products yield distribution are shown in Figures 17, 18, and 19 and the absolute average deviation values are depicted in Table 11. It can be seen that the simulation model of the biochar and water yield distribution correlates better with experimental data of Agblevor et. al. [35] particularly at temperatures 450 and 500°C (AAD < 3%). At temperature 400 °C, water yield in the simulation is 12.3% while in the experiment is 11.3% resulting the AAD about 8.85%. Correlation between the model and experimental data reported by Agblevor et. al. [35] was found to be satisfactory for bio-oil and gas yield results at different pyrolysis temperatures in the range of 400 – 500°C showing that the AAD is lower than 4.2%. However, the overall AAD values of products yields at temperatures 400, 450 and 500 °C are 4.78%, 3.27% and 2.56%, respectively and the global AAD value comes out to be 3.54%.

Based on the previously described statistical analysis, it was discovered that the model was valid for three temperatures and could be confidently utilized for economic analysis at these temperatures.

Table 11. Absolute average deviation (e) for different temperatures

Product	*e* (%) 400°C	*e* (%) 450°C	*e* (%) 500°C
Bio-oil	3.28	4.17	2.79
Biochar	5.02	2.66	2.64
Gas	1.87	3.64	3.70

Water	8.96	2.64	0.14
Overall	4.78	3.27	2.56
Global		3.54%	

As shown in Figs. 17-19, bio-oil yield decreases when the temperature increases from 400 to 450 °C and remains practically constant up to 500 °C while the gas yield increases with the temperature and the biochar yield decreases. The water content in the liquid product increases with the temperature up to 450 °C and decreases up to 500 °C. This result can be explained by the triggering of the secondary vapor cracking reactions such as decarboxylation, decarbonylation, ketonization and cracking of bio-oil to produce pyrolysis water and gas under red mud catalyst effect. In addition, the decrease in the pyrolysis water content at 500°C may be explained by the effect of the catalyst which starts the water gas shift reaction. Compared with the simulation results for non-catalytic pyrolysis in the range of 450-500 °C, the decrease of the biochar yield is due to thermal decomposition effect.

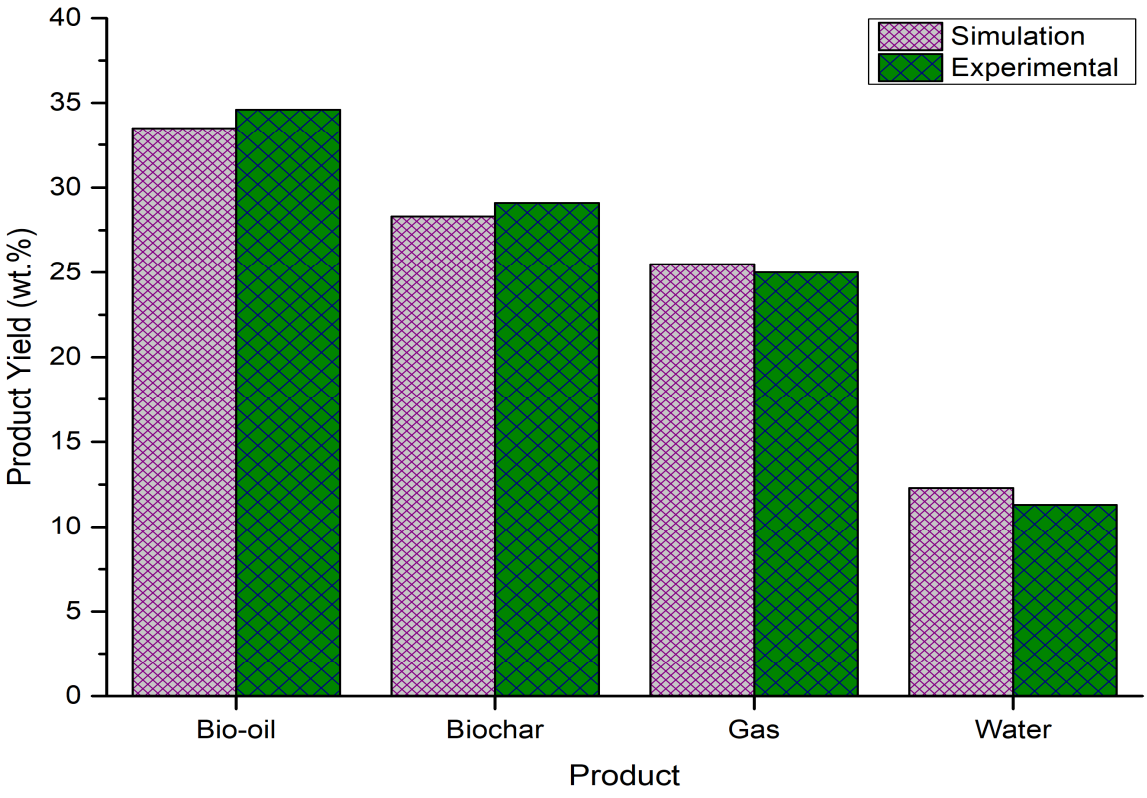

Figure 17. Comparison between simulation and experimental yields at 400°C

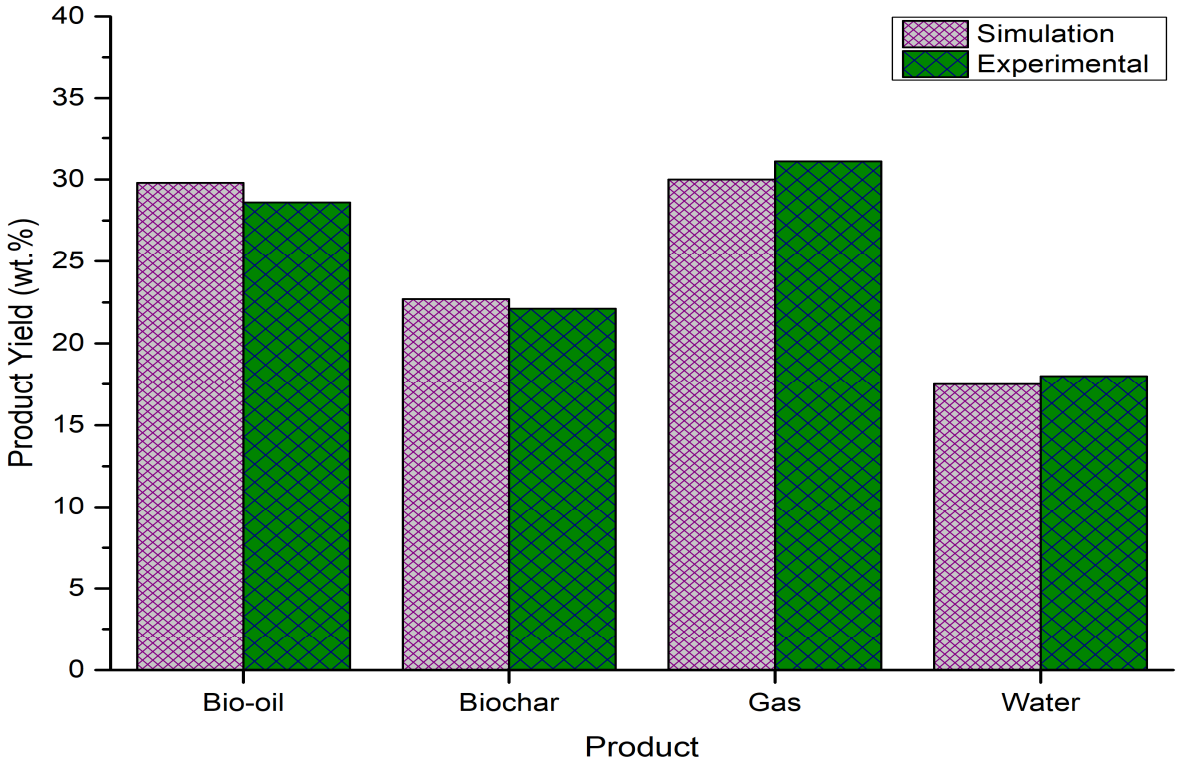

591

592 **Figure 18.** Comparison between simulation and experimental yields at 450°C

593

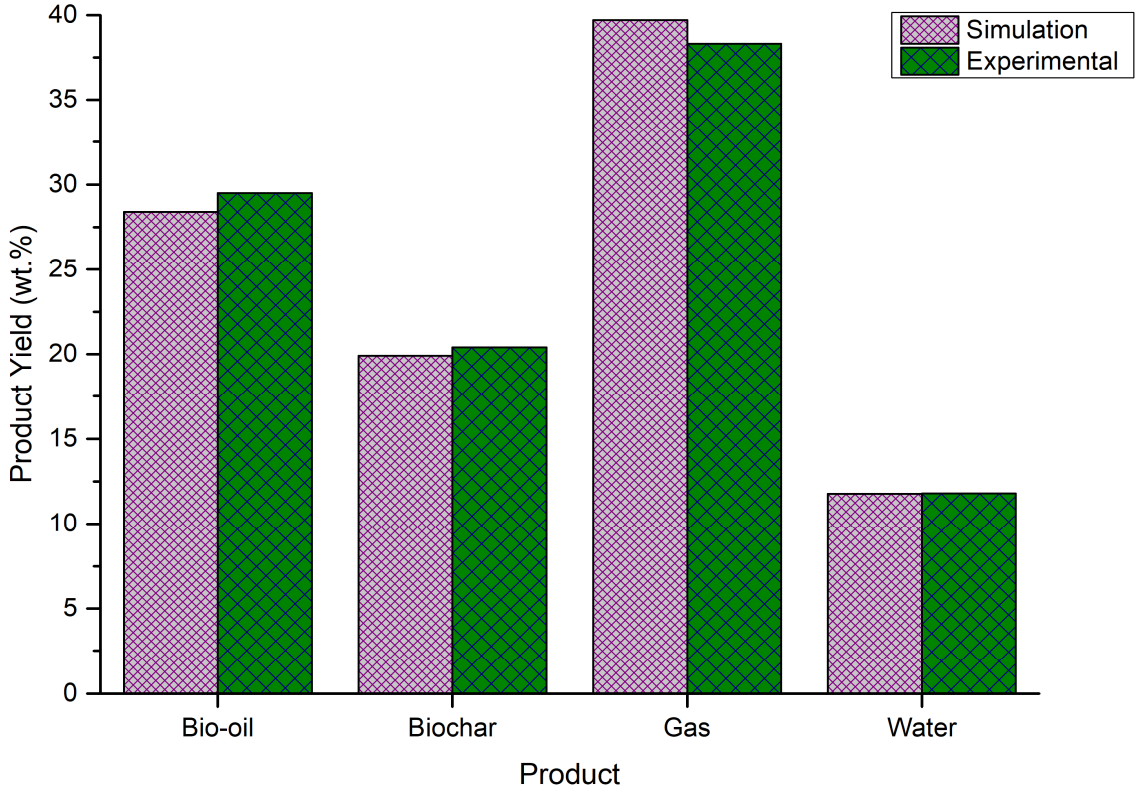

594

595 **Figure 19.** Comparison between simulation and experimental yields at 500°C

596

The composition of fast catalytic pyrolysis product gases predicted from Aspen plus-based simulation was also investigated and compared with the experimental data. The distribution of the gas composition with different pyrolysis temperatures is shown in Figure 20. It can be observed that the model predictions were found to correlate well with experimental data for each gas species at different pyrolysis temperatures. Similar gas species are reported by non-catalytic fast pyrolysis simulations but have different yields under the red mud catalyst effect. As shown in Figure 20a-c, the yield of CO_2 decreased from 78% at 400°C to 66.1% at 500°C whereas the CO, H_2, and CH_4 increased from 6.45%, 2.1%, and 1.6% at 400 °C to 11.8% 3.9% and 3.8% at 500 °C, respectively.

606

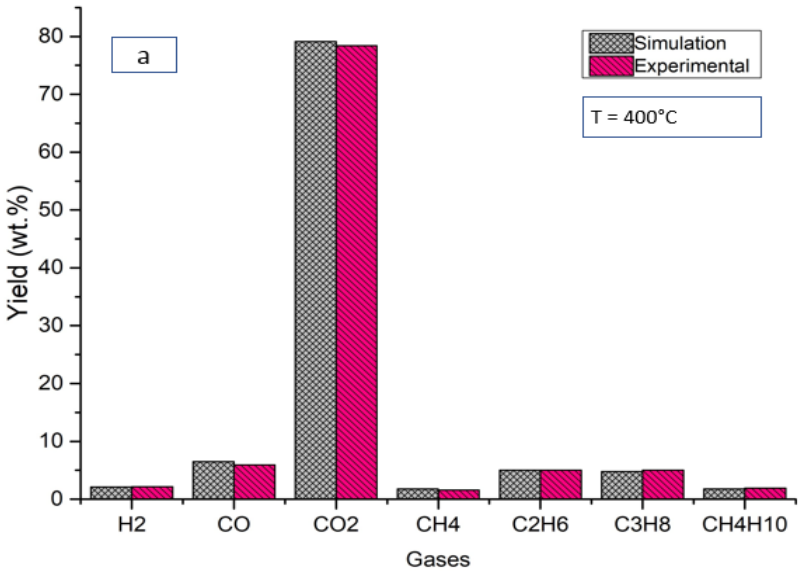

607

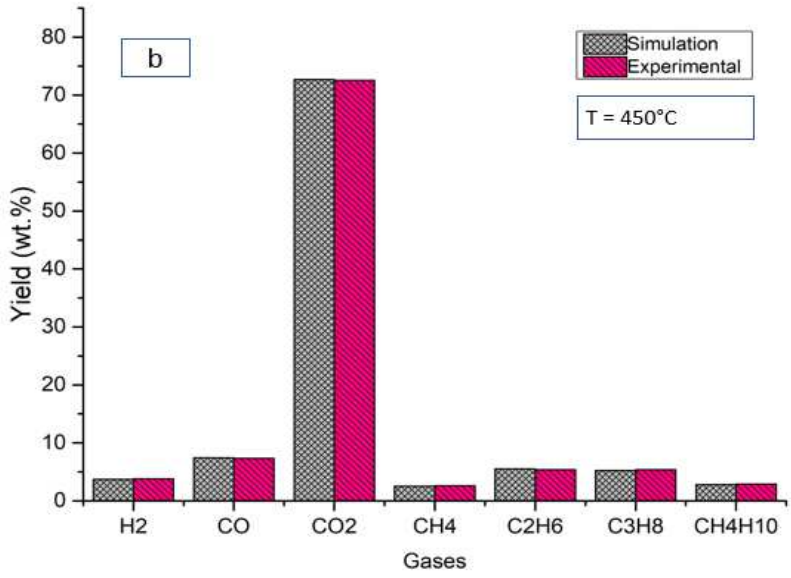

608

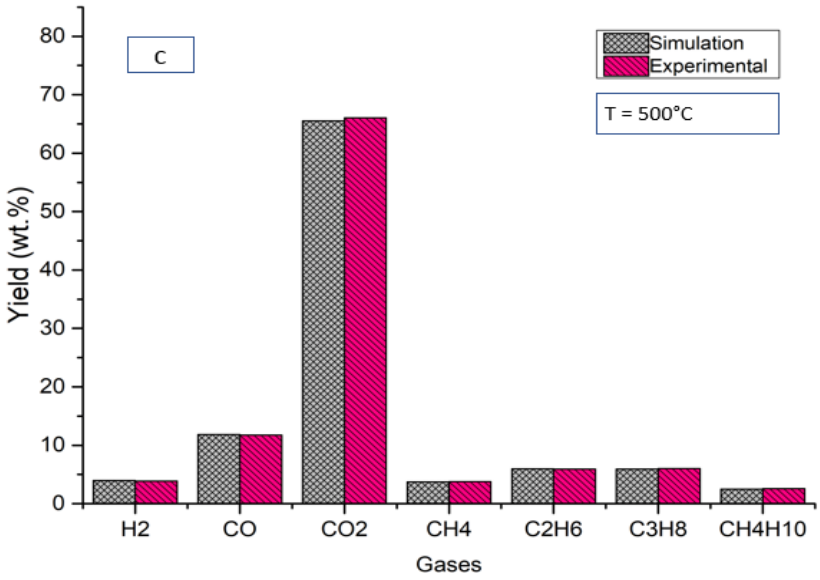

609 **Figure 20.** Gas composition of OMWS for catalytic pyrolysis

610 Figure 21 shows the composition distribution of catalytic bio-oil obtained at 450 °C. It
611 can be seen that the deviations between the model predictions and the experimental data are
612 noticeable for all bio-oil compositions. These deviations are due to the fact that apart from a
613 large number of compounds determined, there is still about 30% of bio-oil composition that
614 could not be determined experimentally. In addition, there are some compounds that could not
615 be found in the Aspen Plus directory so they were termed as unknown compounds. So, this
616 validation is attributed to the limitation of the model to simulate the compounds yields which
617 are present in the catalytic bio-oil.
618

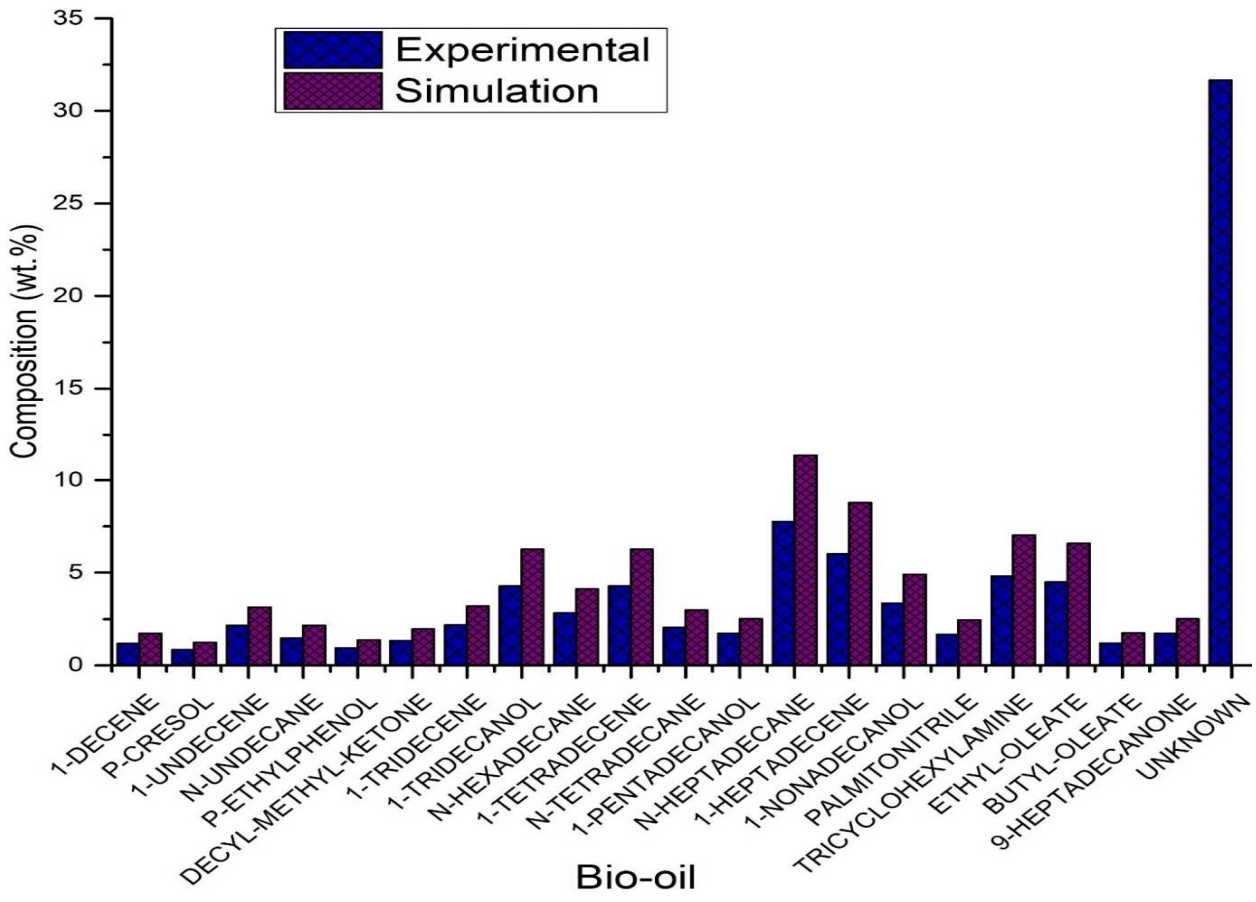

619

620 **Figure 21**. Composition of bio-oil for catalytic fast pyrolysis at 450 °C.

3.2- Techno-economic Assessment

3.2.1- Process performance

The model processed 4,166 kg/h of wet OMWS and produced bio-oil at a rate of 1,366 kg/h. Biochar was combusted to supply heat for the pyrolysis reactions and electricity production in an integrated steam cycle. As a result, the bio-oil production portion (Area 200) is self-sufficient in terms of energy and does not require additional utility heating [16]. In addition, Area 700 produced 603 kW of power. Since the reactor temperature for both process schemes was set to 400°C, there is no difference in fuel yields between the two process schemes. According to experimental results published by Agblevor et. al. [35], the same reactor yields were presumed for both schemes. Nonetheless, the two models vary in terms of electric power usage and capital costs. The discrepancy in energy efficiencies can be explained by the fact that the two systems used different amounts of electricity. In Section 3.2, the economic ramifications of the marginal difference in measured energy efficiencies are assessed. The mass and energy balances derived from the Aspen Plus simulation of the process are shown in Table 12.

Table 12. Mass and energy per hour basis

Process inputs	
Biomass (kg/h)	4,166
Electricity (kWh)	391
Process outputs	
Bio-oil (kg/h)	1,383
Biochar (kg/h)	1,168
NCG (kg/h)	1,012
Water vapors	343
Electricity (kWh)	603

637 *3.2.2- Economic analysis*

638 Figure 22 shows the comparison between proportions of total capital investment for the
639 industrial scale pyrolysis plant for both schemes. The pyrolysis unit accounted for the
640 maximum cost (about €7.10 million) while solids separation section constitutes the minimum
641 capital cost (about €0.15 million). Overall, the total capital cost of the process is estimated to
642 be €22.1 million for scheme-1 and €17.5 million for scheme-2. The higher capital cost
643 observed in scheme-1 compared to scheme-2 is attributable to cost of vapor compression
644 refrigeration machine which is significantly bigger than absorption refrigeration machine.

645

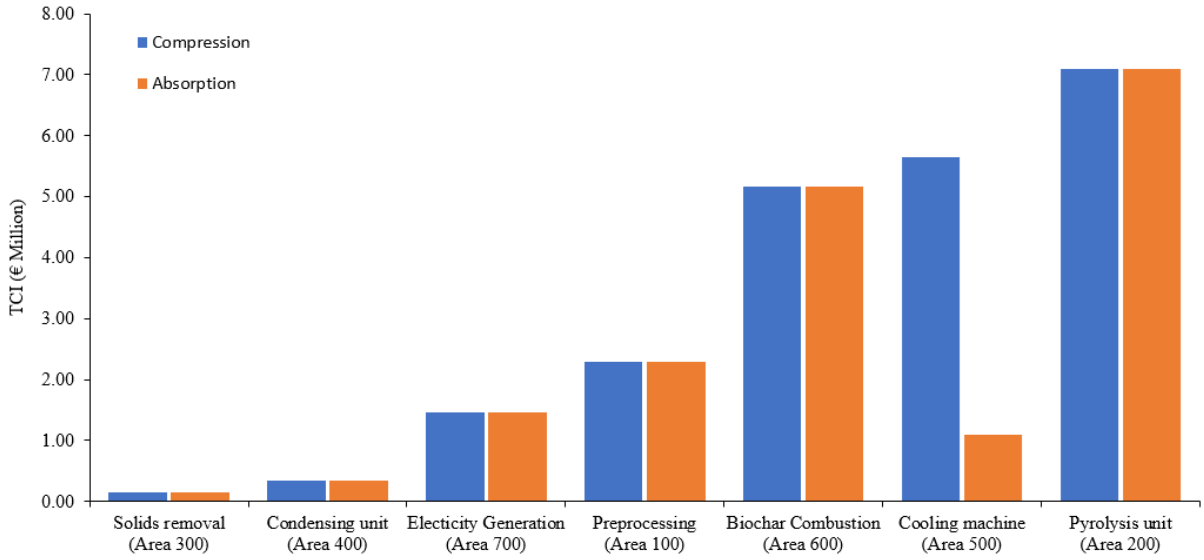

646

647 **Figure 22.** Total capital investment proportions for both schemes

648 The total operating costs of scheme-1 and scheme-2 were estimated at €4.9 million and €3.6
649 million respectively. Figure 23 depicts the allocation of the two designs' constituent operating
650 costs. The higher operating cost in scheme-1 compared to scheme-2 is due to the compression
651 refrigeration machine's comparatively higher electricity usage. Table 13 states the cash flow
652 of the process.

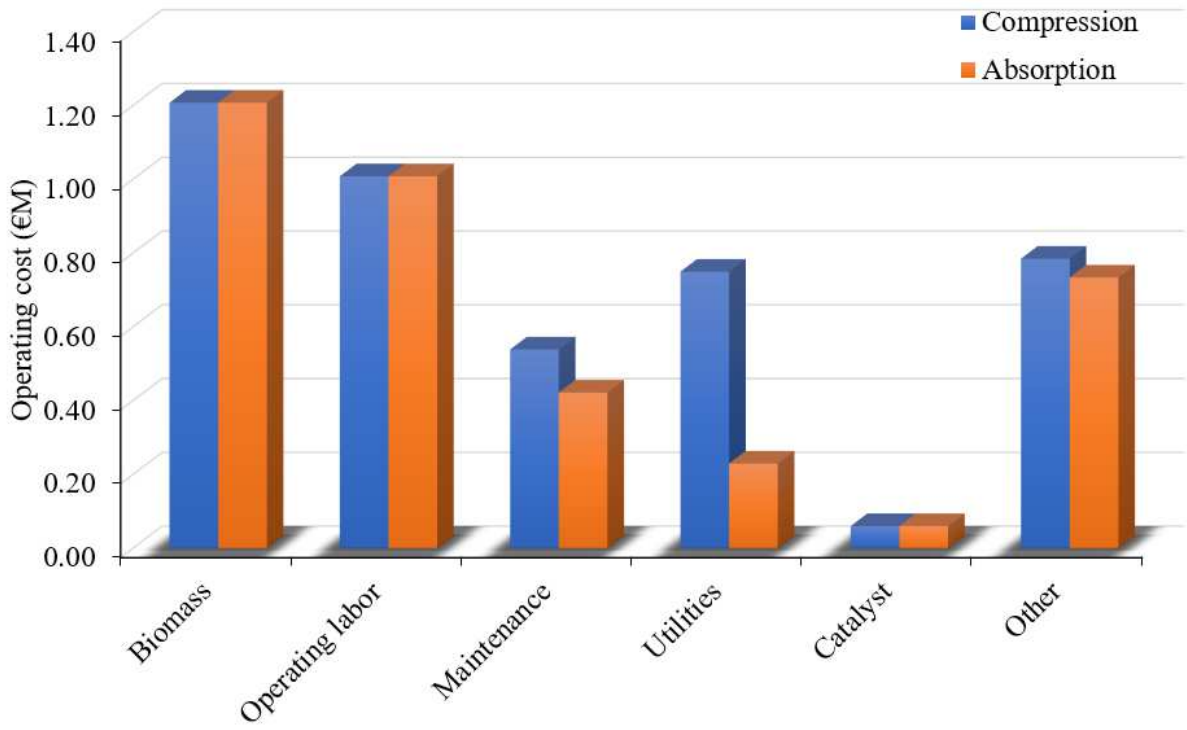

Figure 23. Operating cost proportions

Table 13. Cash flow of the process.

Item	Unit	Value
Number of Weeks per Period	Weeks/period	46.8
Number of Periods for Analysis	Period	20
Base year		2018
Duration of EPC Phase	Period	0.40
Duration of EPC Phase and Startup	Period	2.40
Working Capital Percentage	Percent/period	5
Operating Charges	Percent/period	25
Plant Overhead	Percent/period	50
Total Project Cost	Cost	1.79E+07
Total Raw Material Cost	Cost/period	1.21E+06
Total Operating Labor and Maintenance Cost	Cost/period	9.85E+05
Total Utilities Cost	Cost/period	674,706
Desired Rate of Return/Interest Rate	Percent/period	20

		5
ROR Annuity Factor		
Tax Rate	Percent/period	40
ROR Interest Factor		1.2
Economic Life of Project	Period	20
Salvage Value (Percent of Initial Capital Cost)	Percent	20
Depreciation Method		Straight Line
Project Capital Escalation	Percent/period	5
Products Escalation	Percent/period	5
Raw Material Escalation	Percent/period	3.5
Operating and Maintenance Labor Escalation	Percent/period	3
Utilities Escalation	Percent/period	3
Start Period for Plant Startup	Period	1
Desired Return on Project for Sales Forecasting	Percent/period	10.5
End Period for Economic Life of Project	Period	20
General and administrative Expenses	Percent/period	8
Duration of EP Phase before Start of Construction	Period	0.19
Total Operating Labor Cost	Cost/period	9.07E+05
Total Maintenance Cost	Cost/period	78,203

3.2.3- Sensitivity analysis

The impact of 30% difference in parameters listed in Table 8 was analyzed on the MFSPs of the two process schemes. The effect of variations in these parameters on the MFSP of scheme-1 and scheme-2 can be seen in the sensitivity charts in Figs. 24 and 25. The grey bars depict how sensitive base MFSPs are to a 30% rise in the parameters, while the blue bars portray how sensitive the base MFSPs are to a 30% decrease in the parameters. In general, the longer the bars, the more sensitive the base MFSPs are to parameter changes, and vice versa. Due to the marginal disparity in their capital and operational costs, and similarly in fuel

yields, the MFSPs of both process schemes display equal sensitivities to parameter variations, as seen in Figs. 24 and 25.

A 30% reduction in fuel yield resulted in a 42% increase in MFSP for scheme-1 and a 39% increase in MFSP for scheme-2 (scheme-1: €4.64; scheme-2: €3.81). In contrast, a 30% rise in fuel yield resulted in a 23% decrease in MFSP for scheme-1 and a 21% decrease in MFSP for scheme-2 (scheme-1: €2.49; scheme-2: €2.05). This means that yield losses, which can occur as a result of events like operating and servicing issues, will hurt the profitability of both process schemes.

Scaling up the plant capacity, on the other hand, would be more commercially profitable for both process schemes. Increased plant capacity is one way to increase fuel yield, but it will give rise in capital and operating costs. Both designs' MFSPs were also moderately sensitive to changes in their operating costs. A 30% rise in operating costs resulted in a 18% increase in the MFSP for scheme-1 and a 16% increase in the MFSP for scheme-2 (scheme-1: €3.85; scheme-2: €3.18). In contrast, a 30% reduction in operating costs resulted in MFSP reductions of 19% for scheme-1 and 21% for scheme-2 (scheme-1: €2.64; scheme-2: €2.16). Since biomass feed costs account for a large portion of the running expense, as seen in Fig. 23, finding a less expensive option would be a safer economic decision. Variations in income tax had a major impact on the profitability of both method schemes.

A 30% rise in income tax resulted in a 49% and 46% increase in MFSPs of scheme-1 and scheme-2 respectively (scheme-1: €4.87; scheme-2: €4.01), while a 30% decline in income tax resulted in 33% and 23% decrease in MFSPs of scheme-1 and scheme-2 respectively (scheme-1: €2.16; scheme-2: €1.78). This means that income tax reductions or deductions would be beneficial to the two operation schemes' profitability. As compared to the parameters discussed above, the MFSPs demonstrated less exposure to capital cost, with a 30% rise in capital cost triggering a 11% increase in scheme-1 and an 8% increase in scheme-2 (scheme-1:

691 €3.61; scheme-2: €2.96), and vice versa (scheme-1: €2.88; scheme-2: €2.38). The small impact
692 of higher capital investment on MFSPs, compared to the strong impact of higher bio-oil yield,

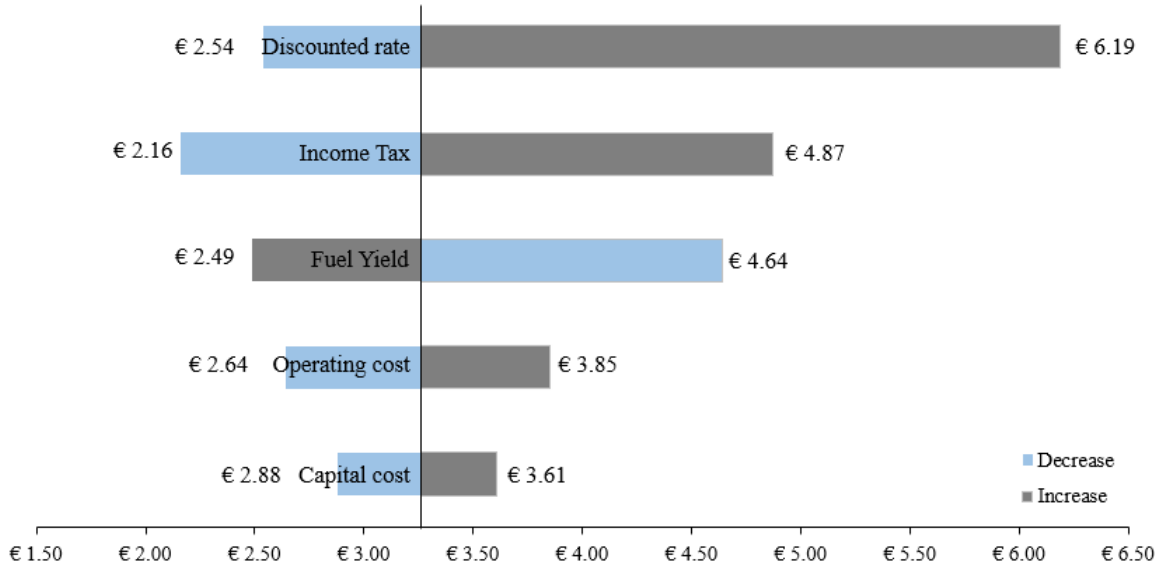

693 indicates that the profitability could be scaled up by increasing plant capacity.
694
695 **Figure 24.** Sensitivity analysis of MFSP
696

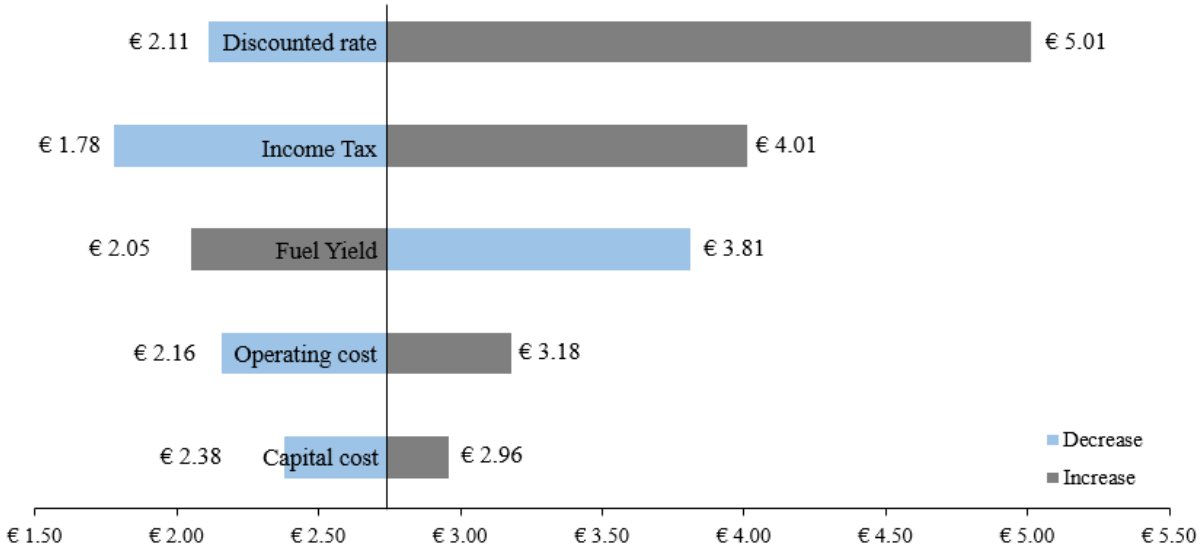

697
698 **Figure 25.** Scheme-2: Sensitivity of MFSP
699 The above sensitivity analysis considered only single point variation of a parameters
700 on MFSP while other parameters were kept constant. To understand the variation of more

than one parameter at a time, a Monte Carlo sensitivity analysis was performed using ModelRisk software [54]. In the Figures 26 and 27, a spider chart has been created to analyze the sensitivity of the mean of the MFSP. Spider plots describe how sensitive the value of an output variable is to the input variable of the model. The horizontal axis shows the cumulative percentile of the economic parameters and the vertical axis shows the mean for the MFSP if the studied economic parameter value was around the percentile value of the horizontal axis. The horizontal line in the middle marks the mean MFSP. The precision of the percentile depends upon the number of tranches; in this case it is 10. This plot is generated using 10,000 samples so each mean MFSP is calculated from 1,000 samples. Spider plot gives more information about the nature of the relationship between economic variables and MFSP. From the charts, it can be observed that capital cost and operating cost remain close to the mean MFSP line so they are least sensitive to MFSP. On the other hand, discounted rate and income tax cover the largest vertical range indicating that they are the most crucial parameters to be observed. Fuel yield has the similar relationship with MSFP but has slightly less influence. The mean MFSP is calculated to be €3.84/GGE for scheme-1 and €3.17/GGE for scheme-2. As discounted rate and income tax are more likely to remain constant during the life of the

717 plant, so increasing the fuel yield can bring down the MFSP of bio-oil significantly.

718 **Figure 26**. Spider chart for scheme-1

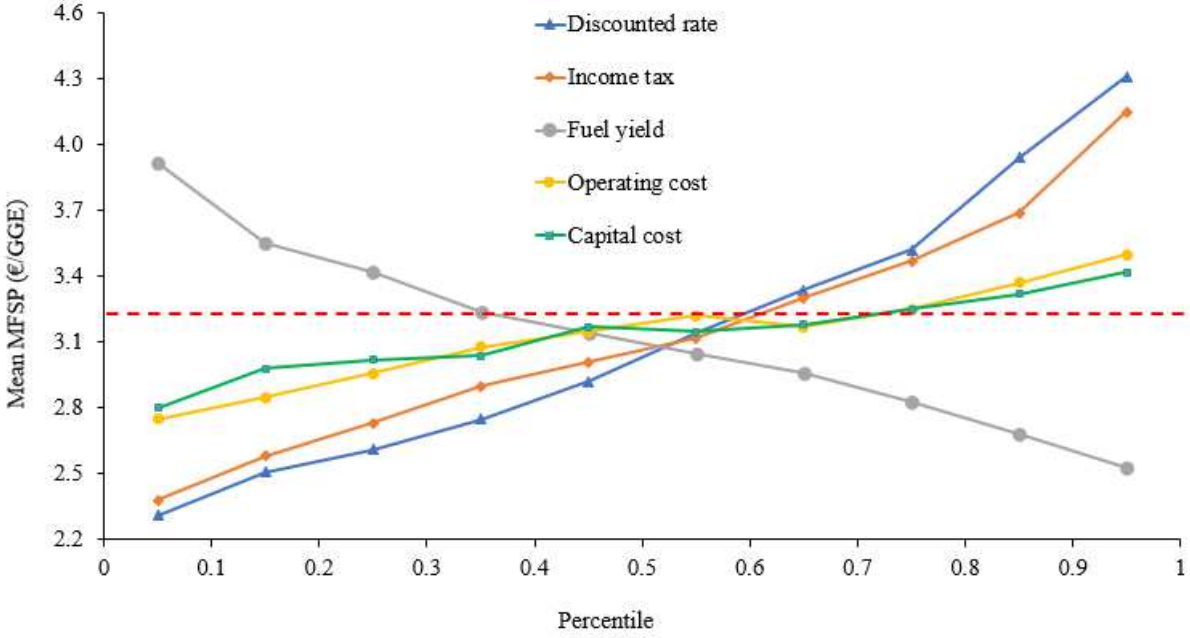

719

720 **Figure 27.** Spider chart for scheme-2

721

722 ## 4- Conclusion

723 A steady state model of pyrolysis of OMWS is developed in Aspen Plus under

724 standard pyrolysis conditions. A global reaction with kinetic parameters is employed in an

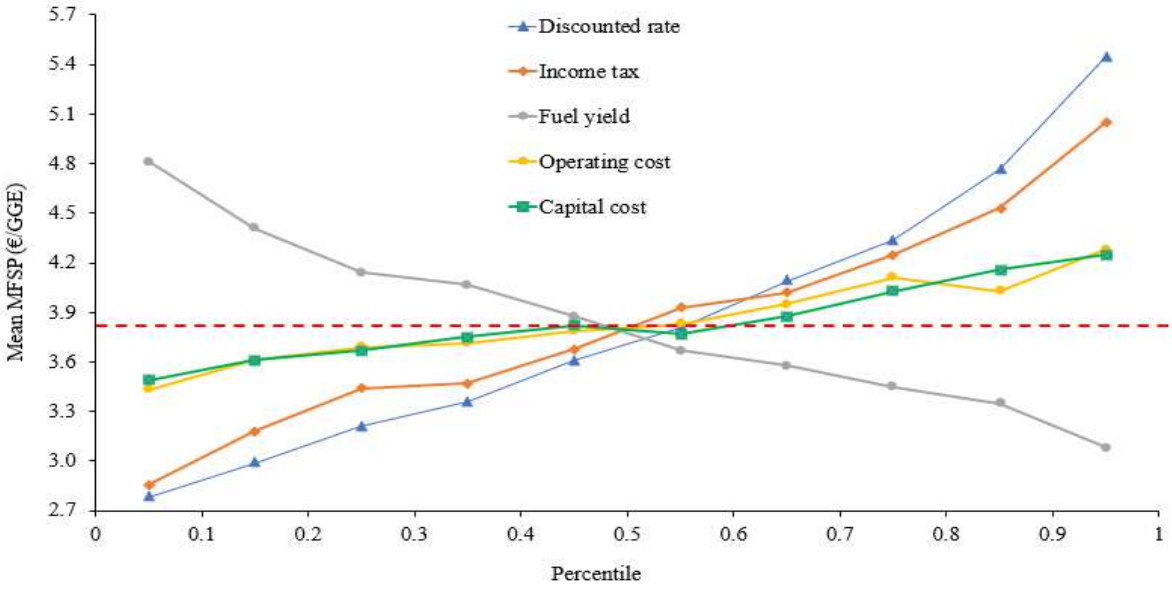

725 external Fortran user-subroutine and coupled with RCSTR reactor. For both catalytic and non-

726 catalytic pyrolysis, a good agreement between simulation and experimental yields can be
727 observed.

728 For non-catalytic pyrolysis, maximum bio-oil yield is obtained at 450°C. Further
729 increase in temperature favors the production of gas and char due to secondary cracking
730 reaction in bio oil vapors thus decreasing the bio-oil yield at higher temperature. Simulation
731 model depicts higher weight percentages of individual bio-oil components to accommodate
732 the unknown compounds present in the bio-oil in experimental data. The prominent gas is
733 CO_2 in the gaseous products comprising of about 81% at 400°C which decreases with rise in
734 temperature. This decrease can be attributed to conversion of CO_2 into CO. Global absolute
735 average deviation of 2.78% is observed for non-catalytic pyrolysis.

736 In the case of catalytic pyrolysis, the optimal temperature for bio-oil production is
737 400°C at which bio-oil is about 34 wt.%. With rise in temperature, decline in bio-oil yield is
738 observed. After 450°C, there is not a significant decrease in bio-oil yield, but gas quantity
739 rises to 38 wt.% which can be regarded to decrease in char yield. For bio-oil, about 31%
740 compounds are unknown in the experimental data so they are compensated with increased
741 contribution from known compounds. Overall AAD for catalytic pyrolysis is about 3.54%.

742 From a technical and economic standpoint, the production of bio-oil from fast pyrolysis
743 of olive mill wastewater sludge has been investigated. In terms of energy consumption and
744 MFSP/GGE, two process schemes (scheme-1 and scheme-2) were examined and compared.
745 The MFSP for scheme-1 is €3.26/GGE, based on a capital investment of €22.1 million and
746 operational expenses of €4.6 million. Scheme-2, on the other hand, had a capital cost of €17.5
747 million and an operating cost of €3.6 million. Scheme-2 had a 0.7 percent higher energy
748 efficiency and a better economic performance than Scheme-1, with a MFSP of €2.74/GGE.
749 Changes in bio-oil yield, operational expenses, and income tax were all equally sensitive to
750 the MFSPs of scheme-1 and scheme-2. According to Monte Carlo sensitivity analysis,

increasing the bio-oil yield could bring the MFSP lower despite increase in capital and operating costs. The profitabilities can be improved considerably with reduction in income tax or exemptions.

Acknowledgments

The authors thank the financial supporters of the Waste2Fuel-ERANETMED2-72-298 collaborative Euro-Mediterranean project. The Tunisian Ministry of Higher Education and Scientific Research, as well as the ANR in France, provided financial and administrative support to the writers. This work is also financed and carried out as a result of international collaboration between University of Loraine, France and University of Sfax, Tunisia under the mechanism of DrEAM within the framework of Lorraine University of Excellence Initiative (LUE).

References

[1] P. Paraskeva, E. Diamadopoulos, Technologies for olive mill wastewater (OMW) treatment: A review, J. Chem. Technol. Biotechnol. (2006). https://doi.org/10.1002/jctb.1553.

[2] N. Sadhwani, S. Adhikari, M.R. Eden, P. Li, Aspen plus simulation to predict steady state performance of biomass-CO2 gasification in a fluidized bed gasifier, Biofuels, Bioprod. Biorefining. (2018). https://doi.org/10.1002/bbb.1846.

[3] A. V. Bridgwater, Review of fast pyrolysis of biomass and product upgrading, Biomass and Bioenergy. (2012). https://doi.org/10.1016/j.biombioe.2011.01.048.

[4] M. Ling, M.J. Esfahani, H. Akbari, A. Foroughi, Effects of residence time and heating rate on gasification of petroleum residue, Pet. Sci. Technol. 34 (2016) 1837–1840. https://doi.org/10.1080/10916466.2016.1230752.

[5] S. Michailos, Kinetic modelling and dynamic sensitivity analysis of a fast pyrolysis fluidised bed reactor for bagasse exploitation, Biofuels. (2018) 1–10. https://doi.org/10.1080/17597269.2018.1461522.

[6] M.I. Jahirul, M.G. Rasul, A.A. Chowdhury, N. Ashwath, Biofuels production through biomass pyrolysis- A technological review, Energies. 5 (2012) 4952–5001. https://doi.org/10.3390/en5124952.

[7] M. Ouadi, J. Brammer, Y. Yang, A.H.-… and applied Pyrolysis, U. 2013, The intermediate pyrolysis of de-inking sludge to produce a sustainable liquid fuel, J. Anal. Appl. Pyrolysis. 102 (2013). https://doi.org/https://doi.org/10.1016/j.jaap.2013.04.007.

[8] S. Elkhalifa, A. AlNouss, T. Al-Ansari, H.R. Mackey, P. Parthasarathy, G. Mckay, Simulation of Food Waste Pyrolysis for the Production of Biochar: A Qatar Case Study, in: Comput. Aided Chem. Eng., Elsevier B.V., 2019: pp. 901–906. https://doi.org/10.1016/B978-0-12-818634-3.50151-X.

[9] A. Dutta, A.H. Sahir, E. Tan, D. Humbird, L.J. Snowden-Swan, P.A. Meyer, J. Ross, D. Sexton, R. Yap, J. Lukas, Process Design and Economics for the Conversion of Lignocellulosic Biomass to Hydrocarbon Fuels: Thermochemical Research Pathways with In Situ and Ex Situ Upgrading of Fast Pyrolysis Vapors, Richland, WA (United States), 2015. https://doi.org/10.2172/1238302.

[10] A. AlNouss, G. Mckay, T. Al-Ansari, Optimum Utilization of Biomass for the Production of Power and Fuels using Gasification, in: Comput. Aided Chem. Eng., Elsevier B.V., 2018: pp. 1481–1486. https://doi.org/10.1016/B978-0-444-64235-6.50258-8.

[11] S. Elkhalifa, A. AlNouss, T. Al-Ansari, … H.M.-C.A., undefined 2019, Simulation of Food waste pyrolysis for the production of biochar: a qatar case study, Elsevier. (n.d.). https://www.sciencedirect.com/science/article/pii/B978012818634350151X (accessed June 12, 2021).

[12] I.A. Vasalos, A.A. Lappas, E.P. Kopalidou, K.G. Kalogiannis, Biomass catalytic pyrolysis: process design and economic analysis, Wiley Interdiscip. Rev. Energy Environ. 5 (2016) 370–383. https://doi.org/10.1002/wene.192.

[13] J.Y. Park, J.K. Kim, C.H. Oh, J.W. Park, E.E. Kwon, Production of bio-oil from fast pyrolysis of biomass using a pilot-scale circulating fluidized bed reactor and its characterization, J. Environ. Manage. 234 (2019) 138–144. https://doi.org/10.1016/j.jenvman.2018.12.104.

[14] J.F. Peters, S.W. Banks, A. V. Bridgwater, J. Dufour, A kinetic reaction model for biomass pyrolysis processes in Aspen Plus, Appl. Energy. 188 (2017) 595–603. https://doi.org/10.1016/j.apenergy.2016.12.030.

[15] I.Y. Mohammed, Y.A. Abakr, R. Mokaya, Integrated biomass thermochemical conversion for clean energy production: Process design and economic analysis, J. Environ. Chem. Eng. 7 (2019). https://doi.org/10.1016/j.jece.2019.103093.

[16] M.B. Shemfe, S. Gu, P. Ranganathan, Techno-economic performance analysis of biofuel production and miniature electric power generation from biomass fast pyrolysis and bio-oil upgrading, Fuel. 143 (2015) 361–372. https://doi.org/10.1016/j.fuel.2014.11.078.

[17] K. Onarheim, Y. Solantausta, J. Lehto, Process simulation development of fast pyrolysis of wood using aspen plus, Energy and Fuels. 29 (2015) 205–217. https://doi.org/10.1021/ef502023y.

[18] J.F. Peters, F. Petrakopoulou, J. Dufour, Exergetic analysis of a fast pyrolysis process for bio-oil production, Fuel Process. Technol. 119 (2014) 245–255. https://doi.org/10.1016/j.fuproc.2013.11.007.

[19] M. Patel, A.O. Oyedun, A. Kumar, R. Gupta, What is the production cost of renewable diesel from woody biomass and agricultural residue based on experimentation? A comparative assessment, Fuel Process. Technol. 191 (2019) 79–92. https://doi.org/10.1016/j.fuproc.2019.03.026.

[20] M. Patel, A.O. Oyedun, A. Kumar, R. Gupta, What is the production cost of renewable diesel from woody biomass and agricultural residue based on experimentation? A comparative assessment, Fuel Process. Technol. 191 (2019) 79–92. https://doi.org/10.1016/j.fuproc.2019.03.026.

[21] E. Ranzi, A. Cuoci, T. Faravelli, A. Frassoldati, G. Migliavacca, S. Pierucci, S. Sommariva, Chemical kinetics of biomass pyrolysis, Energy and Fuels. 22 (2008) 4292–4300. https://doi.org/10.1021/ef800551t.

[22] A. Khosravanipour Mostafazadeh, O. Solomatnikova, P. Drogui, R.D. Tyagi, A review of recent research and developments in fast pyrolysis and bio-oil upgrading, Biomass Convers. Biorefinery. 8 (2018) 739–773. https://doi.org/10.1007/S13399-018-0320-Z.

[23] Y. Zeng, B. Zhao, L. Zhu, D. Tong, C.H.-R. Advances, U. 2013, Catalytic pyrolysis of natural algae from water blooms over nickel phosphide for high quality bio-oil production, RSC Adv. (2013).

[24] T. Aysu, A. Sanna, Nannochloropsis algae pyrolysis with ceria-based catalysts for production of high-quality bio-oils, Bioresour. Technol. 194 (2015) 108–116. https://doi.org/10.1016/J.BIORTECH.2015.07.027.

[25] Y. Yang, J.G. Brammer, M. Ouadi, J. Samanya, A. Hornung, H.M. Xu, Y. Li, Characterisation of waste derived intermediate pyrolysis oils for use as diesel engine fuels, Fuel. 103 (2013) 247–257. https://doi.org/10.1016/J.FUEL.2012.07.014.

[26] M. Tripathi, J.N. Sahu, P. Ganesan, Effect of process parameters on production of biochar from biomass waste through pyrolysis: A review, Renew. Sustain. Energy Rev. 55 (2016) 467–481. https://doi.org/10.1016/J.RSER.2015.10.122.

[27] J. Alvarez, M. Amutio, G. Lopez, J. Bilbao, M. Olazar, Fast co-pyrolysis of sewage sludge and lignocellulosic biomass in a conical spouted bed reactor, Fuel. 159 (2015) 810–818. https://doi.org/10.1016/J.FUEL.2015.07.039.

[28] V. Anand, V. Sunjeev, R. Vinu, Catalytic fast pyrolysis of Arthrospira platensis (spirulina) algae using zeolites, J. Anal. Appl. Pyrolysis. 118 (2016) 298–307. https://doi.org/10.1016/J.JAAP.2016.02.013.

[29] Q. Xu, X. Ma, Z. Yu, Z. Cai, A kinetic study on the effects of alkaline earth and alkali metal compounds for catalytic pyrolysis of microalgae using thermogravimetry, Appl. Therm. Eng. 73 (2014) 357–361. https://doi.org/10.1016/J.APPLTHERMALENG.2014.07.068.

[30] X. Dong, Z. Chen, S. Xue, J. Zhang, J. Zhou, Y. Liu, … Y.X.-R., U. 2013, Catalytic pyrolysis of microalga Chlorella pyrenoidosa for production of ethylene, propylene and butene, RSC Adv. (2013).

[31] M.N. Islam, F.N. Ani, Techno-economics of rice husk pyrolysis, conversion with catalytic treatment to produce liquid fuel, Bioresour. Technol. 73 (2000) 67–75. https://doi.org/10.1016/S0960-8524(99)00085-1.

[32] M. Shemfe, S. Gu, B. Fidalgo, Techno-economic analysis of biofuel production via bio-oil zeolite upgrading: An evaluation of two catalyst regeneration systems, Biomass and Bioenergy. 98 (2017) 182–193. https://doi.org/10.1016/j.biombioe.2017.01.020.

[33] M.M. Wright, D.E. Daugaard, J.A. Satrio, R.C. Brown, Techno-economic analysis of biomass fast pyrolysis to transportation fuels, Fuel. 89 (2010) S2–S10.

https://doi.org/10.1016/j.fuel.2010.07.029.

[34] A. Dutta, J.A. Schaidle, D. Humbird, F.G. Baddour, A. Sahir, Conceptual Process Design and Techno-Economic Assessment of Ex Situ Catalytic Fast Pyrolysis of Biomass: A Fixed Bed Reactor Implementation Scenario for Future Feasibility, Top. Catal. 59 (2016) 2–18. https://doi.org/10.1007/s11244-015-0500-z.

[35] F. Aryi Agblevor, H. Abdellaoui, K. Halouani, S. Hakis Beis, Pyrolytic Conversion of Olive Mill Wastewater Sludge to Biofuels Using Red Mud as Catalyst, Int. J. Energy Power Eng. 6 (2017) 108. https://doi.org/10.11648/j.ijepe.20170606.14.

[36] AspenTech, Aspen Plus user models, (n.d.). https://www.aspentech.com/en.

[37] A.G. Adeniyi, J.O. Ighalo, M.K. Amosa, Modelling and simulation of banana (Musa spp.) waste pyrolysis for bio-oil production, Biofuels. (2019). https://doi.org/10.1080/17597269.2018.1554949.

[38] J. Ward, M.G. Rasul, M.M.K. Bhuiya, Energy recovery from biomass by fast pyrolysis, in: Procedia Eng., Elsevier Ltd, 2014: pp. 669–674. https://doi.org/10.1016/j.proeng.2014.11.791.

[39] J.F. Peters, D. Iribarren, J. Dufour, Predictive pyrolysis process modelling in Aspen Plus ®, in: Researchgate.Net, Copenhagen, 2014. https://doi.org/10.5071/21stEUBCE2013-2CV.4.8.

[40] N. Gautam, A. Chaurasia, Study on kinetics and bio-oil production from rice husk, rice straw, bamboo, sugarcane bagasse and neem bark in a fixed-bed pyrolysis process, Energy. 190 (2020) 116434. https://doi.org/10.1016/j.energy.2019.116434.

[41] A.T. Talwalkar, IGT/DOE coal-conversion systems technical data book, 1981.

[42] R.L. Diaz, J C; Braun, Process simulation model for a staged, fluidized-bed oil-shale retort with lift-pipe combustor (Technical Report) | OSTI.GOV, 1984.

[43] AspenTech, Aspen Plus model for oil shale retorting process, (2010).

[44] C. Somers, A. Mortazavi, Y. Hwang, R. Radermacher, P. Rodgers, S. Al-Hashimi, Modeling water/lithium bromide absorption chillers in ASPEN Plus, Appl. Energy. 88 (2011) 4197–4205. https://doi.org/10.1016/j.apenergy.2011.05.018.

[45] R. Reid, J. Prausnitz, B. Poling, The properties of gases and liquids, (1987). https://www.osti.gov/biblio/6504847 (accessed May 27, 2021).

[46] ASHRAE, Handbook-fundamentals, 1997.

[47] N. Grioui, K. Halouani, A. Zoulalian, F. Halouani, Thermochemical modeling of isothermal carbonization of thick wood particle - Effect of reactor temperature and wood particle size, Energy Convers. Manag. 48 (2007) 927–936. https://doi.org/10.1016/j.enconman.2006.08.003.

[48] Cost Indices, (n.d.). https://www.toweringskills.com/financial-analysis/cost-indices/.

[49] France electricity prices, September 2020 | GlobalPetrolPrices.com, (n.d.). https://www.globalpetrolprices.com/France/electricity_prices/ (accessed April 26, 2021).

[50] TUNISIA - 2021 Finance Law - BDO, (n.d.). https://www.bdo.global/en-

gb/microsites/tax-newsletters/corporate-tax-news/issue-58-april-2021/tunisia-2021-finance-law.

[51] R.E.W. Max S. Peters, Klaus D. Timmerhaus, Plant design and economics for chemical engineers, 5th ed., McGraw-Hill, 2003.

[52] A. Pattiya, J.O. Titiloye, A. V. Bridgwater, Evaluation of catalytic pyrolysis of cassava rhizome by principal component analysis, Fuel. 89 (2010) 244–253. https://doi.org/10.1016/j.fuel.2009.07.003.

[53] F. Paviet, F. Chazarenc, M. Tazerout, Thermo chemical equilibrium modelling of a biomass gasifying process using ASPEN pLUS, Int. J. Chem. React. Eng. 7 (2009). https://doi.org/10.2202/1542-6580.2089.

[54] Risk Analysis Software for Excel | Vose Software, (n.d.). https://www.vosesoftware.com/products/modelrisk/.